

# **Temporal Shifts in the Geochemistry and Microbial Community Structure of an Ultradeep Mine Borehole Following Isolation**

**D. P. MOSER**  
**T. C. ONSTOTT**

Department of Geosciences  
Princeton University  
Princeton, New Jersey, USA

**J. K. FREDRICKSON**  
**F. J. BROCKMAN**

Environmental Microbiology Group  
Pacific Northwest National Laboratory  
Richland, Washington, USA

**D. L. BALKWILL**  
**G. R. DRAKE**

Department of Biomedical Sciences Biology  
Florida State University  
Tallahassee, Florida, USA

**S. M. PFIFFNER**  
**D. C. WHITE**

Center of Biomarker Analysis  
University of Tennessee  
Knoxville, Tennessee, USA

Received 16 May 2002; accepted 8 October 2002.

This research was supported by grants from the National Science Foundation LExEn program (EAR-9714214) and the National Geographic Society (6339-98) with additional travel and support also provided by DOE-OBBER. We gratefully acknowledge the support of Gold Fields Ltd., Driefontein Consolidated Mine, the Universities of Witwatersrand and Orange Free State, and Rob Wilson and colleagues of SRK-Turgis (Pty) Ltd. George Rose of Princeton University designed and constructed the sampling equipment. Aaron Peacock at the University of Tennessee extracted and analyzed the samples for membrane lipid composition. Dawie Nel, Driefontein Chief Geologist, deserves special commendation for assistance with experimental design, underground access, and technical review of the manuscript.

Address correspondence to Duane P. Moser, Pacific Northwest National Laboratory, Environmental Microbiology Group, 902 Battelle Blvd., Mailstop 7-50, P.O. Box 999, Richland, WA 99352, USA. E-mail: duane.moser@pnl.gov

**K. TAKAI**

Subground Animalculae Retrieval (SUGAR) Project  
Frontier Research Program for Deep-Sea Environments  
Japan Marine Science & Technology Center  
Yokosuka, Japan

**L. M. PRATT****J. FONG**

Department of Geological Sciences  
Biogeochemical Laboratories  
Indiana University  
Bloomington, Indiana, USA

**B. SHERWOOD LOLLAR****G. SLATER**

Department of Geosciences  
University of Toronto  
Toronto, Canada

**T. J. PHELPS**

Environmental Sciences Division  
Oak Ridge National Laboratory  
Oak Ridge, Tennessee, USA

**N. SPOELSTRA**

Driefontein Consolidated Mine  
Carletonville, South Africa

**M. DEFLAUN**

Geosyntec  
Princeton, New Jersey, USA

**G. SOUTHAM**

Department of Earth Sciences  
University of Western Ontario  
London, Ontario, Canada

**A. T. WELTY**

Department of Geology  
Northern Arizona University  
Flagstaff, Arizona, USA

**B. J. BAKER**

Department of Geological Sciences  
University of Wisconsin  
Madison, Wisconsin, USA

**J. HOEK**

Department of Earth and Environmental Science  
University of Pennsylvania  
Philadelphia, Pennsylvania, USA

*A borehole draining a water-bearing dyke fracture at 3.2-km depth in a South African Au mine was isolated from the open mine environment. Geochemical, stable isotopic, nucleic acid-based, and phospholipid fatty acid (PLFA) analyses were employed as culture-independent means for assessing shifts in the microbial community and habitat as the system equilibrated with the native rock-water environment. Over a two-month period, the pH increased from 5.5 to 7.4, concurrent with a drop in pe from -2 to -3. Whereas rDNAs related to Desulfotomaculum spp. represented the major clone type encountered throughout, lipid biomarker profiling along with 16S rDNA clone library and terminal restriction fragment length polymorphism (T-RFLP) analyses indicated the emergence of other Gram-positive and deeply-branching lineages in samples during the later stages of the equilibration period. A biofilm that formed on the mine wall below the borehole produced abundant rDNAs related to the  $\alpha$  Proteobacteria.  $\beta$ - and  $\gamma$ -Proteobacteria appeared to transiently bloom in the borehole shortly after isolation. Chemical modeling and sulfur isotope analyses of the borehole effluent indicated that microbial sulfate reduction was the major terminal electron-accepting process shortly after isolation, whereas  $\text{Fe}^{+3}$  reduction dominated towards the end of the experiment. The persistence of Desulfotomaculum-like bacteria throughout suggests that these organisms adapted to changing geochemical conditions as the redox decreased and pH increased following the isolation of the borehole from the mine atmosphere. The restoration of anaerobic aquatic chemistry to this borehole environment may have allowed microbiota indigenous to the local basalt aquifer to become more dominant among the diverse collection of bacterial lineages present in the borehole.*

**Keywords** anaerobic, borehole, community structure, deep subsurface, fissure water, mine

**Introduction**

The existence of a microbial biosphere in the terrestrial deep subsurface is well established (Stevens et al. 1993; Fredrickson and Onstott 1996; Colwell et al. 1997; Pedersen et al. 1997; Pedersen et al. 2000). The current understanding of deep subsurface microbial ecology is founded largely on samples extracted from cores or wells drilled from the surface (Y. Liu et al. 1997; Onstott et al. 1998; Orphan et al. 2000; Chapelle et al. 2002), from rock and water samples obtained from caves (Boston et al. 2001) or mines (Kieft et al. 1997), or boreholes within mines (Kotelnikova and Pedersen 1998; Haveman et al. 1999). While surface drilling embodies advantages of access and well control, only caves and mines enable the direct inspection of intact geological strata in situ prior to the establishment of sampling sites.

Tunnels and ore haulages in the precious metal mines of South Africa access geological strata from 0.8 to 3.5 km below the surface, a depth range for which little is known about subsurface microbiology. Microbial existence at these depths is potentially water- and pore

space-limited due to a predominance of low permeability rock types coupled with temporal and spatial isolation from meteoric inputs. Fracture- and dyke-associated porosities represent the dominant fluid flow pathways and may define the major microbial habitats. While drilling fluids contaminate borehole surfaces in hard rock mines, Pedersen et al. (1997) have reported that even high levels of introduced microbes fail to persist *in situ*. The unidirectional flow of anaerobic groundwater into a mine through a capped or upflowing borehole may reestablish redox conditions and other habitat variables reflective of the source and favor indigenous microorganisms.

As part of ongoing investigations to probe microbial communities and biogeochemical processes of the deep terrestrial biosphere, we investigated microbial community structure and geochemical properties relating to a brine-bearing, dyke-associated fracture in a South African gold mine. The fracture was drained by an unsealed exploratory borehole, which we excluded from mine air in an effort to return the system to a near-undisturbed state. Several complementary, culture-independent approaches were employed to define the boundaries of microbial phylogenetic diversity and determine changes in community structure following this treatment. These data were compared with an analysis of aqueous geochemistry. Here we report the subsequent geochemical shifts, associated phylogenetic succession, and appearance of unusual lineages that resulted from borehole isolation.

## Experimental Procedures

### *Field Site*

The Driefontein Consolidated Mine is located 70 km west of Johannesburg, South Africa (Figure 1a). The deeper levels of 5 Shaft East were chosen for study since these represent the newest and most spatially isolated access tunnels in the area. The study site (Figure 1b) is located at 3,200 meters below land surface (mbls) in the 2.7 Ga Ventersdorp Supergroup, a geologic unit comprised of andesite overlying the actively mined Au-bearing, Carbon Leader horizon within the 2.9 Ga Witwatersrand Supergroup quartzites. The Ventersdorp Supergroup is intruded by dykes and unconformably overlain by dolomite of the Chuniespoort Group. The dolomite contains a partially dewatered aquifer, whereas the Ventersdorp Supergroup is generally dry at this location with the exception of occasional dyke- and fault-associated brines. The predicted virgin rock temperature of the Ventersdorp Supergroup at 3200 mbls in this region, based upon surface heat flow and measured thermal conductivities, is 50°C (Nicolaysen et al. 1981).

The 120-m borehole studied here was diamond-drilled with a 5° deflection into the tunnel wall and a 1° incline in September of 1996. The hole was set with a steel casing (49 mm I.D.) for 2 m into the exposed face and unlined beyond. During drilling, pressurized water was encountered at a location corresponding to a fracture within a known cross-cutting dyke. The tunnel/fracture intersection continues to seep in association with partially cemented fault breccias some 11 m down-tunnel from the borehole outlet. After the initial intersection event, the borehole drained for several weeks, eventually stabilizing at the present flow rate of ca. 1 L/h. At the time of sampling, evaporitic mineral crusts had formed at the outlet and extended back into the hole. Fracture-associated fluids, the overlying dolomite aquifer, and the mine's service water distribution system represent the major potential water sources underground.

### *Sampling, Cartridge Installation, and Sample Processing*

Five samples provided the basis for this study (see Table 1). Water from the mouth of borehole and a biofilm that had accumulated below the borehole were sampled on 11/12/98

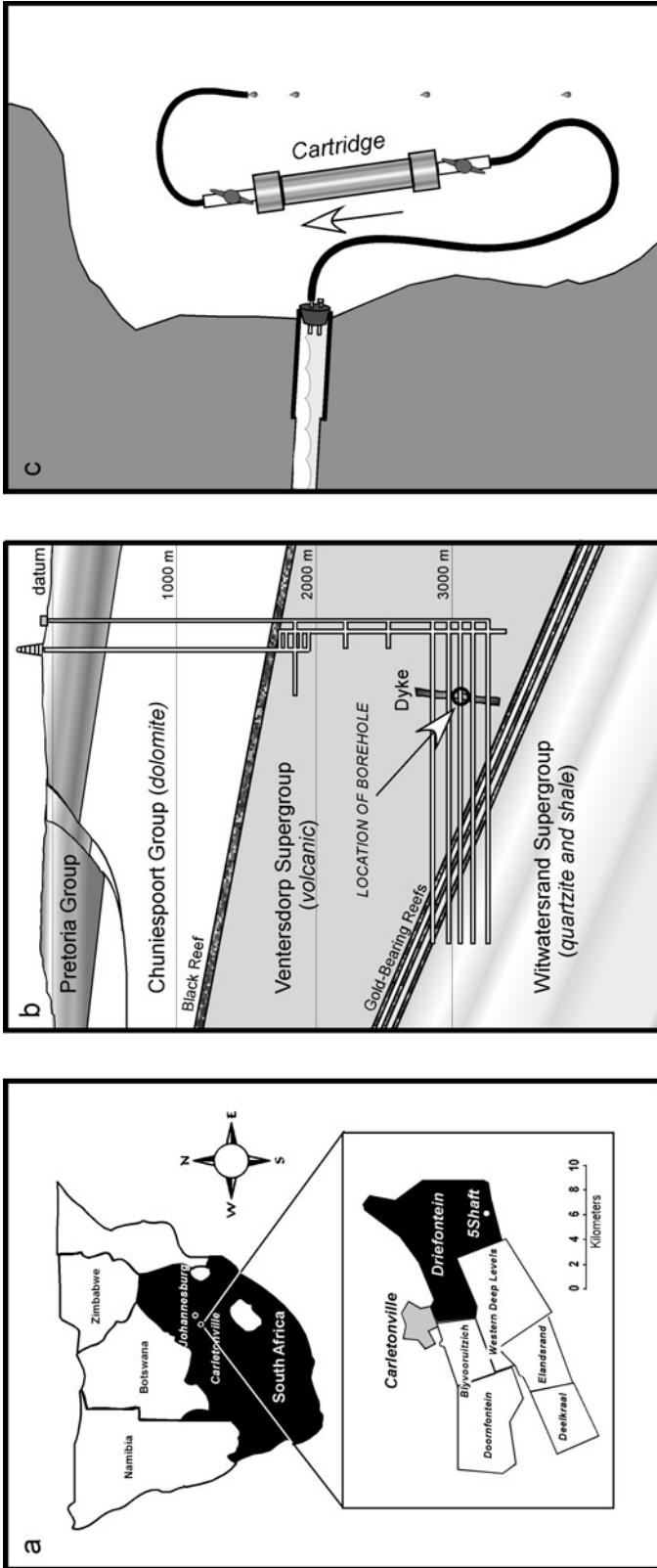


**FIGURE 1** (a) Location of the study site. South Africa and the Driefontein Consolidated Mine property are depicted in black. (b) Geostratigraphy of the sampling site. Mine shafts are shown in simplified form. The location of the borehole is denoted by arrow and circle on 46 level. The levels appear one over another in this cross-sectional view. In reality they are staggered and at the time of the study, there had been no mining directly above the sampling site. (c) Simplified drawing of the experimental setup. Fissure water pooled behind the stopper at the mouth of the borehole and was directed, in an upflow manner, through the cartridge assembly. The cartridge contained locally sourced quartzite rock chips as a physical substrate for microbial colonization. Panels 1a and 1b adapted from Driefontein Consolidated Mine report to shareholders.

**TABLE 1** Samples and analysis summary

Sample	Sample type	Collection date	Analysis performed		
			Chemistry	PLFA	rDNA <sup>a</sup>
1	Borehole water	11/12/98	+	+	
2	Borehole water	12/07/98	+	+	+
3	Borehole water	2/02/99	+	+	+
4	Cartridge material	2/02/99		+	+
5	Biofilm at borehole outlet	11/12/98			+

<sup>a</sup>Clone library and T-RFLP analysis.

(samples #1 and #5, respectively). The borehole was sealed, a water sample collected, and a cartridge experiment (see later) installed. The seal was ported at two positions vertically separated by 2.5 cm, causing water to collect behind the capped lower fitting between subsequent samplings (12/07/98 and 02/02/99) (samples #2 and #3). The overflow was diverted through an autoclaved PVC cartridge (500 ml volume) containing locally sourced quartzite fragments (roughly pea-sized) to provide surfaces for microbial colonization. This assembly was incubated in situ until 02/02/99, when sample #3 and the cartridge (sample #4) were collected. Pooled borehole water was obtained anaerobically via the lower stopper port for subsequent DNA and phospholipid fatty acid (PLFA) analyses in autoclaved, Ar-filled 12.6 L stainless steel canisters (Cornelius, Inc., Anoka, MN, USA).

The cartridge was processed in a glove bag (Coy Laboratory Products, Inc., Grass Lake, MI, USA) with an atmosphere of N<sub>2</sub>:H<sub>2</sub> (98:2). Portions of the cartridge substrate were stabilized by freezing either under N<sub>2</sub> (for PLFA analysis) or with a 5 M guanidineisothiocyanate solution (GIT; Cary et al. 1997) for subsequent DNA analysis. For DNA extraction from borehole water, cells were collected by pressure filtration (N<sub>2</sub> propellant) on 47-mm polysulfone filters (0.22 μm, Supor, Gelman). Filtration for PLFA analysis was performed using methanol-rinsed Anodisc filters (0.2 μm, Whatman, Laguna Niguel, CA, USA) and a baked glass vacuum filtration system (Millipore). All filters were stored at -20°C in the field, transported on dry ice, and subsequently stored at -70°C until analyzed.

### *On-Site Measurements and Collection of Water for Chemical Analysis*

Physical measurements and samples for water chemistry were collected from the lower stopper port. Temperature was measured using a digital thermometer (Fisher brand) and pH, a Piccolo pH Meter (Hanna Instruments Inc., Woonsocket, RI, USA), verified against litmus test strips. Oxidation/reduction potential (redox) was measured with an Orion platinum electrode (Orion Research Inc., Beverly, MA, USA) and the instrument readout corrected according to Zobell (1946). All collection bottles were triple-rinsed with nanopure H<sub>2</sub>O and oven-dried prior to the addition of preservatives.

Dissolved anion samples were filtered (22-μm Nylon Acrodisk, Gelman) into 50-ml polypropylene bottles (Nalgene). Cation, dissolved ammonia, and dissolved iron samples were likewise filtered, but preserved with 2.5 ml concentrated HNO<sub>3</sub>, 50 μl concentrated H<sub>2</sub>SO<sub>4</sub>, and 2 ml concentrated HCl, respectively. Unfiltered samples were each collected in their respective bottle type and with the appropriate preservative preloaded: dissolved inorganic carbon (DIC, 300 ml glass "BOD" bottles, 200 μl saturated HgCl<sub>2</sub> preservative); ammonia (20-ml glass vials, 50 μl concentrated H<sub>2</sub>SO<sub>4</sub> preservative); sulfide (45-ml amber glass vials, 500 μl 2N ZnAc preservative); δ<sup>34</sup>S (60-ml plastic syringes, 500 μl 2N ZnAc or 10 ml 2N AgNO<sub>3</sub> as preservative); δD, δ<sup>18</sup>O<sub>2</sub> (15-ml serum bottles, crimp sealed); δ<sup>13</sup>C

and  $^{14}\text{C}$  of DIC, 50-ml amber septum bottles (50  $\mu\text{l}$   $\text{HgCl}_2$  as preservative); dissolved gases including  $\text{H}_2$ ,  $\text{CH}_4$ , and He, 160-ml evacuated serum bottles; dissolved  $\text{O}_2$ , (300-ml glass BOD bottles  $\text{MnSO}_4 + \text{KOH}$  pillows, Hach, Loveland, CO, USA). Formate/acetate samples were collected in 45-ml glass vials with Teflon septa and preserved frozen. Dissolved organic carbon (DOC), total organic carbon (TOC), and volatile organic compounds (VOC) samples were collected in the same vials and preserved with 100  $\mu\text{l}$  of 1:1 concentrated  $\text{HCl}$ :water.

### ***Chemical and Isotopic Analyses***

Cation,  $\text{Br}^-$ , and  $\text{I}^-$  concentrations were measured by inductively coupled plasma-mass spectrometry (ICP-MS, Activation Laboratories Ltd., Ontario, Canada). Total P was determined by inductively coupled plasma-atomic emission spectroscopy (ICP-AES, Perkin-Elmer Instruments, Shelton, CT, USA).  $\text{F}^-$ ,  $\text{Cl}^-$ ,  $\text{Br}^-$ , nitrate, nitrite, sulfate, and phosphate were determined by ion chromatography (Dionex, Sunnyvale, CA, USA). DIC was determined by infrared spectrophotometry (Johnson et al. 1987). The  $\delta^{34}\text{S}$  of sulfide and sulfate were determined by combusting the  $\text{ZnS}$  and  $\text{BaSO}_4$  at high temperature to  $\text{SO}_2$  followed by isotope ratio mass spectrometry analysis. The  $\delta^{13}\text{C}$  of inorganic carbon was determined by isotope ratio mass spectrometry (Mountain Mass Spectrometry, Evergreen, CO, USA) from  $\text{CO}_2$  released by phosphoric acid. The  $\delta^{18}\text{O}$  of the water was determined by equilibration with  $\text{CO}_2$  of known isotopic composition and then analyzed by isotope ratio mass spectrometry (Mountain Mass Spectrometry, USA). The  $\delta\text{D}$  was determined by high temperature reduction of water on Zn followed by isotope ratio mass spectrometry analysis (Environmental Isotopes Laboratory, University of Waterloo, Waterloo, Ontario) of the resulting  $\text{H}_2$  gas.

The ammonia concentration was determined according to Standard Methods (Eaton et al. 1995). Organic carbon was measured from acidified samples as  $\text{CO}_2$  generated by catalytic combustion (EPA Method # 415.1) using an infrared detector (Tekmar Dohrman DC-190, Perkin-Elmer). For the measurement of dissolved organic carbon, the sample was centrifuged at  $10,000 \times g$  for 10 min and the supernatant analyzed. Acetate and VOCs were measured by gas chromatography using a Restek 30-meter Stabilwax column and a Varian 3400 equipped with a flame ionization detector (EPA Method 8015). Formate was measured by ion chromatography using a Dionex Ion Pac AS4A-SC 4-mm column and conductivity detector (EPA Method 300). The gas composition was measured by GC coupled to thermal conductivity and flame ionization detectors. The dissolved gas concentrations were then calculated by multiplying the gas composition by the estimated pressure in the borehole and using the Henry's law coefficients for each gas at the borehole temperature.

Geochemical reaction paths (Table 3) were calculated by starting with the composition of borehole sample #2 and modifying that composition with one or more redox reactions in order to simulate the composition of sample #3. The Geochemist's Workbench release 3.2 (Rockware, Inc., Golden, CO, USA) was utilized for modeling the reaction paths. The Thermo.dat database of Wolery et al. (Delaney and Lundeen 1990) was the basis for calculating the equilibrium constants, activity coefficients, and the Eh and pH phase diagrams.

### ***PLFA Analysis***

Total PLFA composition was analyzed using procedures described by White and Ringelberg (1998). After extracting the filters, biofilm, and cartridge material by a modified, single-phase, chloroform-methanol-phosphate buffer procedure (Bligh and Dyer 1959; White et al. 1979), the total extractable lipid was fractionated on a silicic acid column using a

microtechnique (Tunlid et al. 1989). The polar lipid fraction was collected and transesterified into fatty acid methyl esters (FAMES) by mild alkaline methanolysis for gas chromatography/mass spectrometry (GC/MS) analysis (Guckert et al. 1985; White and Ringelberg 1998). The identity of FAMES was verified using GC/MS in comparison with standards (Matreya Inc. Pleasant Gap, PA, USA) using previously published GC/MS conditions (White and Ringelberg 1998; Takai et al. 2001b).

### **Scanning Electron Microscopy**

Samples of the colonized cartridge material were fixed in filled cryovials using 2% (aq) glutaraldehyde in cartridge water and shipped to the United States for analysis. The samples were processed through an ethanol dehydration series (25%, 50%, 75%, and 100%, 100%, 100%–5 min each) followed by a critical point dry in order to preserve the integrity of the bacterial cells and any associated extracellular polysaccharides. Each sample was then gold coated and examined at 15 kV using a LEO-435VP SEM.

### **DNA Extraction and 16S rDNA Amplification**

DNA was extracted from samples using the UltraClean Soil DNA Mega Prep kit (MoBio Laboratories Inc., Solana Beach, CA, USA). Final kit extracts (6 ml) were concentrated by alcohol precipitation in isopropanol/NaOAc (9:1) followed by a 70% ethanol wash (Sambrook, Fritsch, and Maniatis 1989) and resuspension in 11  $\mu$ l H<sub>2</sub>O. Small subunit rRNA genes (SSU rDNAs) were amplified using TaKaRa LA Taq polymerase (Panvera, Madison, WI, USA) using provided buffers, dNTPs and reaction mixtures containing oligonucleotide primers at 0.4  $\mu$ M and template 50 ng/ $\mu$ l. Thermal cycling employed a GeneAmp 9600 (Perkin Elmer): denaturation at 96°C, 30 sec; annealing at 50°C, 45 sec; and extension at 72°C, 2 min for 35 cycles. For rDNA libraries, oligonucleotide primers 27f (*Eubacteria*-specific; Giovannoni 1991) and 907r (universal; Lane 1991) were used. For terminal restriction fragment length polymorphism (T-RFLP) analysis, primer 27f was labeled with 5'-tetrachlorofluorescein (PE Applied Biosystems). Archaeal PCR was performed using 21f (DeLong 1992) and Arch915 (Stahl and Amann 1991) or universal 1492r (Lane 1991) primers. PCR products were verified by agarose gel electrophoresis and amplicons purified by excision from gels and use of GelSpin columns (MoBio Laboratories Inc.).

### **T-RFLP**

For restriction fragment analysis of amplified community rDNA (WT Liu et al. 1997), product from three PCR reactions was pooled, electrophoresed, and the excised band purified using a GelSpin column. This labeled rDNA was double digested with 4-bp restriction endonucleases (*Hae*III and *Hha*I) and the terminal restriction fragments (T-RFs) detected using an automated DNA sequencer (model 377) and GeneScan software (ver. 3.0, PE Applied Biosystems). Precise T-RF lengths were determined using an internal size standard (TAMRA 2500, PE Applied Biosystems). Electropherograms were edited manually and the GeneScan data imported into GelCompare II software (ver. 2.5, Applied Maths, Kortrijk, Belgium) with band matching at 0.10% position tolerance. Jaccard and Jaccard area-sensitive coefficients (Sokal and Sneath 1963) were used with the unweighted pair group method (UPGMA; Sokal and Mitchner 1958) to generate dendrograms (Jaccard shown here, Figure 6).

The 16S rDNA clone sequences were digested in silico (DNAsis software package, Hitachi Engineering Software Co.) with the same enzymes used in T-RFLP and the predicted

5' T-RFs compared to those produced by T-RFLP. Major ribotypes were conditionally assigned to T-RF predictions based on compliance with an empirically derived fragment size accuracy criterion. To generate this criterion, portions of an amplified rDNA restriction digest were run across 10 lanes of polyacrylamide gels (separate gels on 2 consecutive days). In the test, 100% of the bands in all lanes matched between the gels and the following standard was established:  $\pm 0.25$  bp for bands  $<320$  bp,  $\pm 0.5$  bp for bands between 320 and 600 bp, and  $\pm 2.0$  bp for bands  $>600$  bp.

### ***Clone Libraries and DNA Sequencing***

PCR products were cloned into pCR2.1 using the Original TA cloning kit (Invitrogen, Carlsbad, CA, USA). Insert-containing *E. coli* clones were treated with Lyse-N-Go reagent (Pierce, Rockford, IL, USA) and aliquots used as template for PCR from M13 primers (Sambrook et al. 1989). Exonuclease I and shrimp alkaline phosphatase (Amersham Pharmacia Biotech, Buckinghamshire, UK) were added and PCR reactions incubated in a thermocycler (37°C for 60 min, then 85°C for 90 min) for the removal of primers and residual dNTPs. PCR products were sequenced directly from primer 27f using the Big Dye sequencing kit and ABI 377 DNA sequencer (PE Applied Biosystems).

### ***Phylogenetic Analysis of Clone Sequences***

The first 450 bases from each clone sequence were analyzed using the Sequence Match feature of the Ribosomal Database Project (RDP II, Maidak et al. 1999) to identify the most similar 16S rRNA sequences in the database. The sequences were then tentatively placed into groups based on their individual relationships to those comprising the RDP databases and therefore likely to represent distinct clone types. A preliminary alignment of the sequences for each clone type was produced by assembling them with the Sequencher program (Sequencher 3.0, Gene Codes Corp., Ann Arbor, MI, USA). All of the clone sequences were then manually edited in the context of 16S rRNA secondary structure (Gutell 1994), checking for correct pairing in double stranded regions and unlikely changes in the length of the sequence in single stranded regions. The GenBank accession numbers for the fully evaluated and edited sequences are: cartridge (sample #4), AF459047 through AF459076; biofilm (sample #5), AF546906 through AF546927; water sample from 12/98 (sample #2), AF546928 through AF546961; water sample from 2/99 (sample #3), AF546962 through AF546991.

The sequences in each putative clone type were manually aligned (taking secondary structure into consideration) to selected comparison sequences from the RDP and GenBank/EMBL and DDBJ databases. Alignments included both the closest database matches as well as less similar sequences for use as outgroups during phylogenetic analyses. In the case of clone types with very low similarity to their nearest database match, alignments included representatives from all of the major divisions of eubacteria designated by the RDP.

Three phylogenetic approaches were used to analyze the aligned sequences: distance matrix, parsimony, and maximum likelihood. PHYLIP (Felsenstein 1993) was used for distance matrix analyses. Distances were calculated by the method of Jukes and Cantor (1969), after which phylogenies were estimated with the algorithm of Fitch and Margoliash (1967). Parsimony analyses were carried out with the PAUP program (PAUP 4.0, beta version 8; Sinauer Associates, Inc., Sunderland, MA, USA), using the standard program defaults for heuristic searches. Maximum likelihood analyses were performed with the DNAML option in PHYLIP or with PAUP, using the standard program defaults. The branch

nodes in the phylogenetic trees generated by distance matrix and parsimony analyses were further evaluated by bootstrapping data at the >50% confidence limits, with 100 replications (Felsenstein 1985). The phylogenetic relatedness of the clones to previously described bacteria and environmental clones was determined by comparison of the results from the three different phylogenetic methods and by evaluation of bootstrap data. The analyses split sequences in some clone types into two or more distinct subtypes. These subtypes were considered to be separate clone types if the distinctions between them were retained in trees produced by all three analytical approaches.

To produce summary trees, selected sequences from the above alignments were placed into two large alignments, the first containing all of the clones that appeared to be members of the *Proteobacteria* and the second containing the remainder. The sequences in each large alignment included one representative from each clone type, the sequences that were most closely related to each clone type (based on the earlier phylogenetic analyses), and additional comparison sequences. The large alignments were then analyzed phylogenetically as described above. Regions of sequence alignment in which data were missing from some of the sequences or the alignment was ambiguous were excluded from the analyses. The first large alignment included sequence corresponding to positions 40–546 in the 16S rRNA sequence for *Escherichia coli* (Brosius et al. 1979). The excluded regions corresponded to positions 70–97, 202–215, and 455–477; 475 bases were retained in the analysis. The second large alignment included sequence corresponding to *E. coli* positions 40–520. The excluded regions corresponded to positions 66–101, 202–215, and 450–483; 422 bases were retained in the analysis. Sequence similarities were calculated only over the regions included in the preceding analyses.

## Results

### *Aqueous Chemical and Isotope Analyses*

Borehole water was saline with total dissolved solids (TDS) ranging from 5.63 wt% in sample #1 to 3.54 wt% and 3.78 wt% in the later samples (#2 and #3, Table 2). The temperature of the borehole effluent increased from 35°C to 37.2°C and the pH first dropped from 6.0 to 5.5 and then climbed to 7.42. Dissolved O<sub>2</sub> remained below detection limits throughout, whereas dissolved H<sub>2</sub> increased from less than 0.03 (detection limit) to 0.9 μM. Dissolved CH<sub>4</sub> increased from 5.4 to 8.2 μM and He decreased from 1.9 to 1.1 μM. Formate and acetate concentrations in sample #2 were below detection (0.016 and 0.0084 mM, respectively).

The δD and δ<sup>18</sup>O stable isotopic signatures of the borehole water differed markedly from those of service and dolomite water sources. δD and δ<sup>18</sup>O values for borehole water samples were –24.387, –13.14, and –12.8, respectively (Table 2). In comparison, the δD values of service and dolomite waters were –8.59 and –20.38; and the δ<sup>18</sup>O values were –2.7 and –4.55 (Takai et al. 2001a). The net result is that the δD vs. δ<sup>18</sup>O positions of both dolomite and service water conform to the global meteoric water line (Takai et al. 2001a), whereas those of the borehole water (Table 2) lie far to the left of it. The δ<sup>34</sup>S of the sulfate and sulfide in sample #2 were +19.2‰ and +1.4‰ CDT, respectively. Significant concentrations of TOC, DOC, and DIC were present in the borehole water (sample #2). The corresponding δ<sup>13</sup>C of DIC in sample #2 was –17.8‰ PDB and the calculated equilibrium pCO<sub>2</sub> was 10<sup>–1.9</sup> atmospheres, a value higher than that of the mine air (S. Kotelnikova, pers. comm., 1999).

Relative proportions of the major cations, Ca<sup>+2</sup>, Na<sup>+</sup>, Sr<sup>+2</sup>, and K<sup>+</sup> did not change, whereas the concentrations of Fe, sulfate, and DIC did. Dissolved iron increased by 0.69 mM

**TABLE 2** Physical and chemical characteristics of borehole waters

	Sample		
	Borehole (#1) 11/12/98	Borehole (#2) 12/7/98	Borehole (#3) 2/2/99
Physical measurements			
Depth (kmbls)	3.21	3.21	3.21
Temp. (°C)	35.0	37.0	37.2
pH	6.00	5.50	7.42
pe	n.a. <sup>a</sup>	-2	-3
Dissolved gases (μM)			
O <sub>2</sub>	n.a.	0.00	0.00
H <sub>2</sub>	n.a.	<0.03	0.9
CH <sub>4</sub>	n.a.	5.4	8.2
He	n.a.	1.9	1.1
Stable isotopes			
δ <sup>18</sup> O‰ (VSMOW)	n.a.	-13.14	-12.80
δD‰ (VSMOW)	n.a.	-24.387	n.a.
δ <sup>13</sup> C‰ DIC (PDB)	n.a.	-17.84	-17.20
δ <sup>34</sup> S‰ sulfate (CDT)	n.a.	19.2	18.7
δ <sup>34</sup> S‰ sulfide (CDT)	n.a.	1.4	n.a.
Organic carbon (mM)			
TOC	n.a.	0.830	n.a.
DOC	n.a.	0.670	n.a.
Formate	n.a.	<0.016	n.a.
Acetate	n.a.	<0.0084	n.a.
Inorganic carbon (mM)			
DIC	n.a.	0.410	.570
Anions (mM)			
F <sup>-</sup>	0.098	0.085	0.100
Cl <sup>-</sup>	2210	1320	1330
Br <sup>-</sup>	2.430	1.330	1.710
NO <sub>3</sub> <sup>-</sup>	n.d. <sup>b</sup>	n.d.	n.d.
SO <sub>4</sub> <sup>-2</sup>	n.a.	0.579	1.160
HS <sup>-</sup>	n.a.	0.036	n.a.
Total P as PO <sub>4</sub> <sup>-3</sup>	0.137	0.492	0.133
Cations (mM) <sup>c</sup>			
Filtered NH <sub>3</sub>	n.a.	0.001	0.029
Unfiltered NH <sub>3</sub>	n.a.	0.044	0.048
Ca	295	233	220
Na	278	248	259
Sr	1.420	1.140	1.260
Fe	1.530	0.514	1.210
K	1.530	1.320	1.440
Si	0.351	0.153	0.314
Li	0.434	0.365	0.402
Ba	0.022	0.016	0.016
Mg	0.074	0.044	0.046

(Continued on next page)

**TABLE 2** Physical and chemical characteristics of borehole waters (*Continued*)

	Sample		
	Borehole (#1) 11/12/98	Borehole (#2) 12/7/98	Borehole (#3) 2/2/99
Rb	0.012	0.0076	0.011
Zn	0.016	n.d.	0.0010
I	0.0052	0.060	0.045
Cs	0.0036	0.0036	0.0030
Ni	0.0048	0.0016	n.d.
Cr	0.0049	n.d.	n.d.
Cu	0.0037	0.0010	n.d.
Mn	0.0042	0.0016	0.0013
Al	0.0047	0.000	0.000
TDS wt/%	5.63	3.54	3.78
Br <sup>-</sup> /Cl <sup>-</sup> molar ratio	0.0026	.0022	.0027
pCO <sub>2</sub>	n.a.	-1.85	-3.24
Saturation Indices			
Calcite	n.a.	-1.66	0.75
Siderite	n.a.	-2.12	0.75
Gypsum	-1.6	-1.26	-0.94
Barite	-0.1	-0.42	0.0
Goethite	n.a.	-1.35	2.81
FeS	n.a.	-0.19	n.a.

<sup>a</sup>n.a.-Not applicable, sample not taken.

<sup>b</sup>n.d.-Not detected.

(from 0.51 mM to 1.2 mM). DIC increased by 0.16 mM and the  $\delta^{13}\text{C}$  of the DIC increased slightly to  $-17.2\text{‰}$  PDB (from  $-17.84\text{‰}$ , Table 2). Sulfate increased in concentration by 0.58 mM (from 0.58 mM to 1.16 mM), while the  $\delta^{34}\text{S}$  of the sulfate decreased slightly from  $19.2\text{‰}$  to  $18.7\text{‰}$  CDT (Table 2). Sample #2 was undersaturated with respect to calcite ( $\text{CaCO}_3$ ) and siderite ( $\text{FeCO}_3$ ), whereas sample #3 was saturated with respect to these two phases (Table 2, Table 3, Figure 2). The pCO<sub>2</sub> decreased to  $10^{-3.2}$  atmospheres during the 2 months of isolation from mine air. The increase in sulfate was sufficient to saturate sample #3 with respect to barite ( $\text{BaSO}_4$ ), but the borehole remained undersaturated with respect to gypsum ( $\text{CaSO}_4$ ). Sample #2 was slightly undersaturated with respect to goethite and FeS (Table 2) and oxidized Fe was observed coating the interior of the borehole's metal casing.

### PLFA Biomarker Analysis

Membrane phospholipids were analyzed in all of the samples (Figure 3). Total PLFA concentrations, a measure of viable microbial biomass, increased in samples #1 to #3 with time. Values ranged from 0.1 pmole/ml in #1, to 2.5 pmole/ml in #2, and 12 pmole/ml in #3. Total phospholipid biomass associated with the quartzite fragments from the cartridge incubated in situ was 2,000 pmole/g and that of the biofilm from below the borehole was 1,800 pmole/g. These concentrations correspond to  $2.5 \times 10^3$  cells/ml for #1, to  $6.25 \times 10^4$  cells/ml for #2, and to  $3 \times 10^5$  cells/ml for #3 using a conversion factor of  $2.5 \times 10^4$  cells/pmole PLFA (Balkwill et al. 1988). Using the same conversion factor, samples from the cartridge material and biofilm contained  $5 \times 10^7$  cells/g and  $4.5 \times 10^7$  cells/g, respectively. These

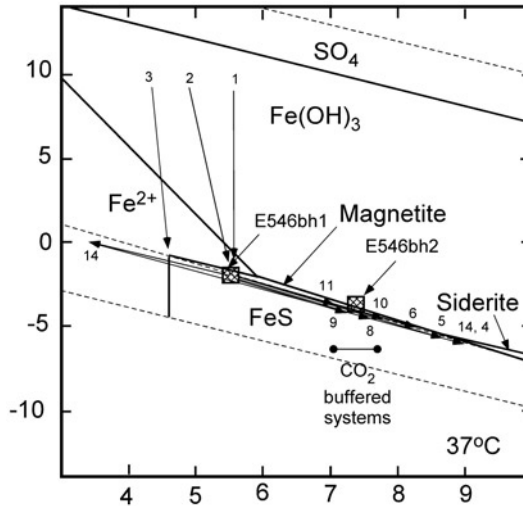


**FIGURE 2** pe vs. pH diagram for Fe (1 mmol), S (1 mmol), and CO<sub>2</sub> (p CO<sub>2</sub> = 0.012 atm) system. Solid lines demarcate mineral stability fields for magnetite, FeS, siderite, and Fe(OH)<sub>3</sub> or HFO. Dashed lines demarcate stability fields for sulfur species. Arrows denote reaction paths for reactions in Table 3. Numbers correspond to numbers in Table 3. The positions of the samples #2 and #3 are indicated.

values, however, are likely not directly comparable due to the much higher bulk proportion of rock in the cartridge sample.

PLFA profiles indicated a shift in microbial community structure following installation of the seal. Overall, most major classes increased in relative abundance at the expense of the normal saturates, which decreased from an initial 76 mol% to 22 to 25 mol% (Figure 3). Normal saturated fatty acids were ubiquitous and their relative mole percentages generally

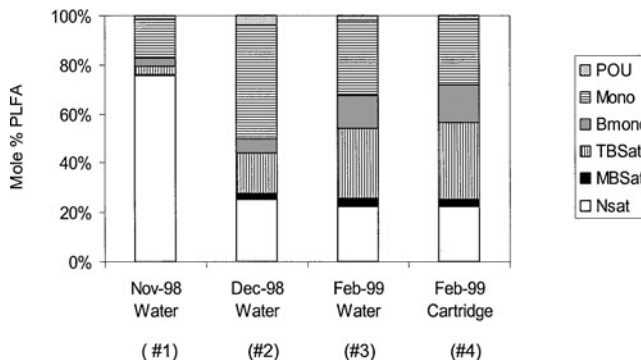


**FIGURE 3** PLFA profiles for borehole water and cartridge samples over time. The borehole seal was inserted between the November and December samplings. Throughout this time course, total PLFA concentrations generally increased. Values ranged from 0.1 pmole/ml in #1, to 2.5 pmole/ml in #2, and 12 pmole/ml in #3. Total phospholipid associated with the cartridge fragments was 2,000 pmole/g. PLFA groupings were normal saturates (Nsat), mid-branched saturates (MBSat), terminally branched saturates (TBSat), branched monounsaturates (Bmono), monounsaturates (Mono), and polyunsaturates, oxirane, and unknown fatty acids (POU).

**TABLE 3** Molar changes noted in borehole water between samples #2 and #3 and possible chemical reactions that might account for them

Sample #2	Sample #3	Molar/change										Concentrations				
		$\Delta\text{H}^+$	$\Delta\text{SO}_4^{2-}$	$\Delta\text{Fe}^{2+}$	$\Delta\text{DIC}$	$\Delta\text{DOC}$	$\Delta\text{HS}^-/\text{H}_2\text{S}$	$\Delta\text{O}_2$	$\Delta\text{H}_2$	pH	pe	$\text{SO}_4^{2-}$	$\text{Fe}^{++}$	DIC	$\delta^{34}\text{S}$	$\delta^{13}\text{C}$
		-3E-06	5E-04	7E-04	1.6E-04	$\leq 7\text{e-}4$	$\leq 7\text{e-}4$	-3E-04	2E-08	5.5	-2	4.80E-04	5.10E-04	4.10E-04	19.2	-17.8
Aerobic reactions																
1)	$\text{H}_2 + 0.5\text{O}_2 = \text{H}_2\text{O}$									7.4	-3 to -4	9.70E-04	1.20E-03	5.70E-04	18.7	-17.2
2)	$\text{CH}_3\text{COO}^- + 2\text{O}_2 = 2\text{HCO}_3^- + \text{H}^+$	0.00E+00	0.00E+00	0.00E+00	0.00E+00	0.00E+00	0.00E+00	-3E-04	-6E-04	5.5	-2	4.80E-04	5.10E-04	4.10E-04	19.2	-17.8
3)	$\text{H}_2\text{S} + 2\text{O}_2 = 2\text{H}^+ + \text{SO}_4^{2-}$	8.00E-05	0.00E+00	0.00E+00	1.6E-04	-1.6E-04	0.00E+00	-1.6E-04	0.00E+00	5.54	-2	4.80E-04	5.10E-04	5.70E-04	19.2	-19.0
		1.00E-03	5.00E-04	0.00E+00	0.00E+00	0.00E+00	5.00E-04	-1E-03	0.00E+00	4.2	-2	9.70E-04	5.1e-04 <sup>d</sup>	4.10E-04	11.1	-17.8
Anaerobic reactions																
4)	$\text{HS}^- + 8\text{Fe}(\text{OH})_3 + 15\text{H}^+ = \text{SO}_4^{2-} + 8\text{Fe}^{2+} + 20\text{H}_2\text{O}$	-1.50E-03	1.00E-04	8.00E-04	0.00E+00	0.00E+00	1.00E-04	0.00E+00	0.00E+00	9.05 <sup>b</sup>	-5.80	5.80E-04	1.30E-03	4.10E-04	16.1 <sup>d</sup>	-17.8
5)	$\text{H}_2 + 2\text{Fe}(\text{OH})_3 + 4\text{H}^+ = 2\text{Fe}^{2+} + 6\text{H}_2\text{O}$	-1.40E-03	0.00E+00	7.00E-04	0.00E+00	0.00E+00	0.00E+00	0.00E+00	3.50E-04	8.75 <sup>b</sup>	-5.25	9.7e-4 <sup>c</sup>	1.00E-03	4.10E-04	19.2	-17.8
6)	$\text{CH}_3\text{COO}^- + 8\text{Fe}(\text{OH})_3 + 15\text{H}^+ = 2\text{HCO}_3^- + 8\text{Fe}^{2+} + 20\text{H}_2\text{O}$	-1.35E-03	0.00E+00	7.00E-04	8.75E-05	8.75E-05	0.00E+00	0.00E+00	0.00E+00	8.2	-4.5	9.7e-4 <sup>c</sup>	1.20E-03	4.98E-04	19.2	-18.5
Anaerobic reactions w/carbonate buffering																
7)	$\text{HS}^- + 8\text{Fe}(\text{OH})_3 + 15\text{H}^+ = \text{SO}_4^{2-} + 8\text{Fe}^{2+} + 20\text{H}_2\text{O} + \text{pCO}_2 = 0.0064$	-1.50E-03	8.75E-05	7.00E-04	2.70E-04	0.00E+00	-8.75E-05	0.00E+00	0.00E+00	7.53	-4.20	5.68E-04	1.20E-03	6.80E-04	16.5	-18.7
8)	$\text{HS}^- + 8\text{Fe}(\text{OH})_3 + 15\text{H}^+ = \text{SO}_4^{2-} + 8\text{Fe}^{2+} + 20\text{H}_2\text{O}$ magnetite $\rightarrow$ siderite	-1.50E-03	1.00E-04	8.00E-04	-2.10E-04	0.00E+00	-1.00E-04	0.00E+00	0.00E+00	7 <sup>b</sup>	-3.80	5.80E-04	1.30E-03	3.60E-04	16.1	-18.1
9)	$\text{H}_2 + 2\text{Fe}(\text{OH})_3 + 4\text{H}^+ = 2\text{Fe}^{2+} + 6\text{H}_2\text{O}$ pCO <sub>2</sub> = 0.0064	-1.40E-03	0.00E+00	7.00E-04	1.60E-04	0.00E+00	0.00E+00	0.00E+00	3.50E-04	7.45	-4.1	9.7e-4 <sup>c</sup>	1.20E-03	5.70E-04	19.2	-18.4
10)	$\text{H}_2 + 2\text{Fe}(\text{OH})_3 + 4\text{H}^+ = 2\text{Fe}^{2+} + 6\text{H}_2\text{O}$ siderite	-1.60E-03	0.00E+00	8.00E-04	-2.20E-04	0.00E+00	0.00E+00	0.00E+00	3.50E-04	7.15 <sup>b</sup>	-3.6	9.7e-4 <sup>c</sup>	1.30E-03	3.50E-04	19.2	-18.2
11)	$\text{CH}_3\text{COO}^- + 8\text{Fe}(\text{OH})_3 + 15\text{H}^+ = 2\text{HCO}_3^- + 8\text{Fe}^{2+} + 20\text{H}_2\text{O}$ pCO <sub>2</sub> = 0.0064	-1.35E-03	0.00E+00	7.00E-04	1.90E-04	-8.75E-05	0.00E+00	0.00E+00	0.00E+00	7.5	-4.2	9.7e-4 <sup>c</sup>	1.20E-03	6.00E-04	19.2	-18.2
12)	$\text{CH}_3\text{COO}^- + 8\text{Fe}(\text{OH})_3 + 15\text{H}^+ = 2\text{HCO}_3^- + 8\text{Fe}^{2+} + 20\text{H}_2\text{O}$ magnetite $\rightarrow$ siderite	-1.50E-03	0.00E+00	8.00E-04	1.90E-04	-1.00E-04	0.00E+00	0.00E+00	0.00E+00	7.0	-3.4	9.7e-4 <sup>c</sup>	1.30E-03	6.00E-04	19.2	-18.6
Anaerobic sulfur cycling																
13)	$\text{HS}^- + 8\text{Fe}(\text{OH})_3 + 15\text{H}^+ = \text{SO}_4^{2-} + 8\text{Fe}^{2+} + 20\text{H}_2\text{O}$ and $2\text{CH}_3\text{COO}^- + \text{SO}_4^{2-} = \text{HS}^- + 2\text{HCO}_3^-$ magnetite	1.50E-03	2.00E-05	8.00E-04	1.60E-04	-1.60E-04	-2.00E-05	0.00E+00	0.00E+00	9	-6	5.00E-04	1.30E-03	5.70E-04	18.5	-19.0

<sup>a</sup> During oxidation, Fe+3 phases would precipitate, lowering Fe until O<sub>2</sub> levels decrease to the point that magnetite or sulfide minerals are stable.

<sup>b</sup> Reaction attained  $\Delta G = 0$ .

<sup>c</sup> Sulfate added by dissolution of gypsum.

<sup>d</sup> The equilibrium  $\delta^{34}\text{S}$  of the H<sub>2</sub>S in the borehole would be 3‰ heavier than that measured for HS<sup>-</sup>.

decreased as biomass increased. Midbranched saturates, indicative of sulfate reducers and/or actinomycetes (Dowling et al. 1986; Vainshtein et al. 1992; Kohring et al. 1994; Boschker et al. 1998), increased from 0.6 mol% in #1 to greater than 3 mol% in samples #3 and #4. Terminally branched saturates, indicative of Gram-positive and some anaerobic bacteria (O'Leary and Wilkinson 1988), increased from 3 mol% in sample #1, to 17 mol% in #2, and further to 28 mol% and 31 mol% in samples #3 and #4. Branched monounsaturates, which may be diagnostic for sulfate and metal reducers (Dowling et al. 1986; Kohring et al. 1994; Nichols et al. 2000) increased from 3 mol% in sample #1, to 5 mol% in sample #2, and ultimately 14 and 16 mol% in samples #3 and #4. Gram-negative bacteria are indicated by the monounsaturates (White et al. 1997). Monounsaturated fatty acids initially comprised 16 mol%, increased to 47 mol% in sample #2, and then decreased to 30.6 and 27 mol% in samples #3 and #4. A major polyenoic PLFA (18:2 $\omega$ 6), indicative of eukaryotes (Findlay and Dobbs 1993; White et al. 1997), was detected in all samples at 0.5–1.6 mol%. The other PLFAs were detected at trace levels. The biofilm sample (#5) was not part of the time progression summarized in Figure 3 and thus considered separately. The PLFA composition of this sample included: normal saturated fatty acids, 18 mol%; midbranched saturates, 1 mol%; terminally branched saturates, 2 mol%; branched monounsaturates, 1 mol%; monounsaturates, 42 mol%; and polyunsaturates, 10 mol%. Free fatty acids, a minor constituent in the other samples, comprised over 26% in sample #5.

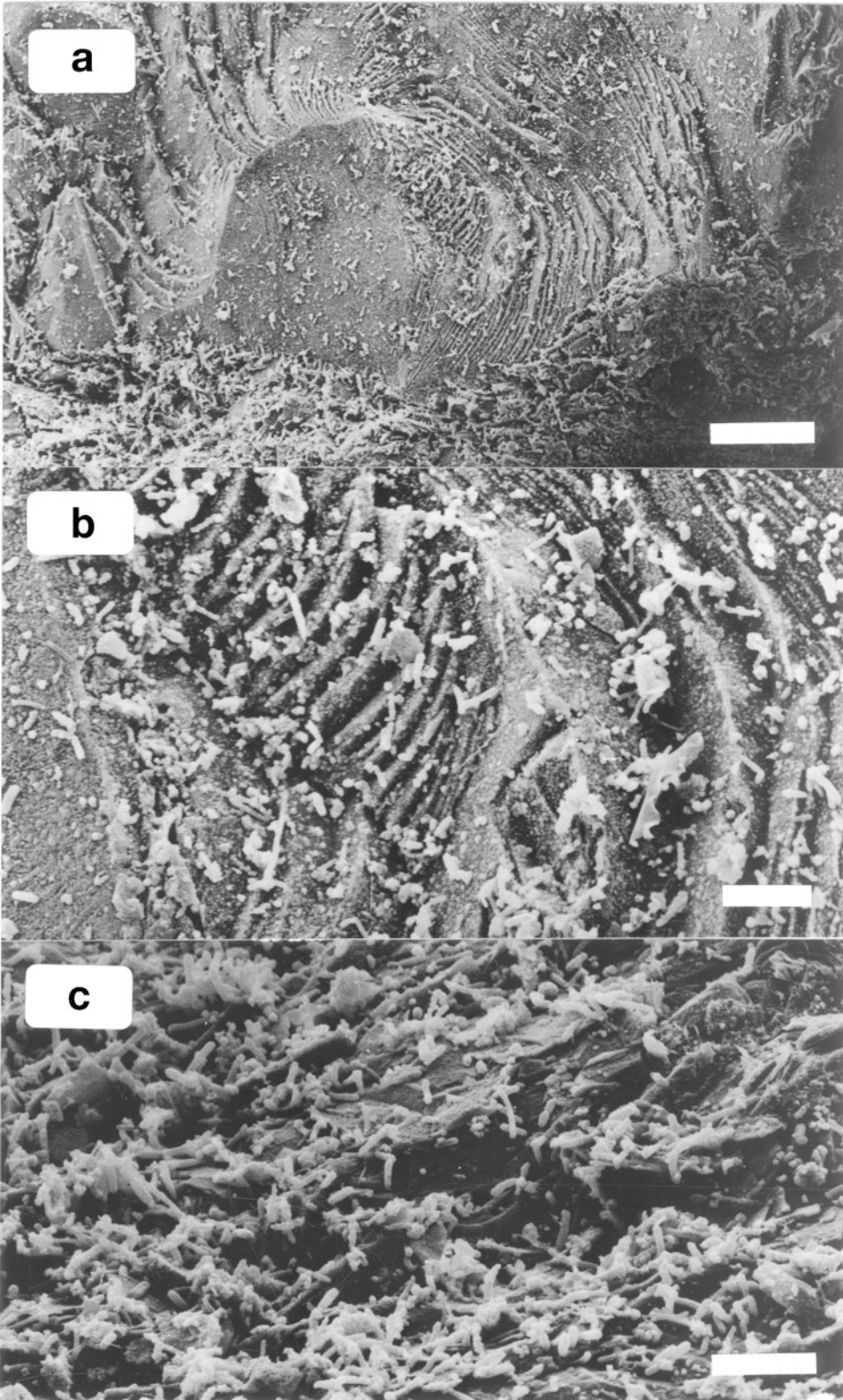
### SEM

Bacterial colonization of the quartzite fragments occurred in a heterogeneous manner (Figure 4a) and did not appear to be controlled by  $\mu$ m-scale surface features (Figure 4b), suggesting that preferential flow paths “around” the fragments controlled the amount of bacterial growth. The depth of the biofilm did not exceed a few  $\mu$ m (Figure 4c). Since this is not deep enough to create a redox boundary within the biofilm, all of the bacteria in the cartridge were exposed to similar chemical conditions. Also, extensive exopolymeric material in association with cells was not evident on the quartzite surfaces.

### T-RFLP Analysis

T-RFLP analysis resolved a total of 40 peaks in sample #2, 45 in #3, 38 in #4, and 41 in #5 (major peaks visible in Figure 5). Since there were many more ribotypes detected in the T-RFLP analysis than clone types in the clone libraries, many of the minor ribotypes were unrepresented in the libraries. The majority of library clone types could, however, be associated with specific potential ribotypes from the T-RFLP gels (Table 4). One notable exception was the strong peak at 259 bp (Figure 5), which appeared in all profiles but whose predicted ribotype failed to be represented in any of the clone libraries. A prominent peak occurring in all samples is consistent with the predicted 264 bp *HaeIII* T-RF of clone type 18. A “C” to “A” base substitution in the first *HaeIII* site of a clone otherwise matching type 18 resulted in the establishment of an additional possible ribotype (here denoted “18a,” Table 4). In type 18a, the first cut site is shifted to the 291 bp position and may thus correspond to a minor peak at that position appearing in all of the profiles (Figure 5).

The biofilm sample yielded peaks corresponding to predicted T-RFs from clone type 6 (82 bp) and 4 (193 bp). The remainder (types 1, 2, 3, and 5) generated predicted T-RFs of 39 bp. In sample #2, a major peak at position 211 bp probably corresponds to the abundant *Marinobacter*-like type 16 clones. Peaks corresponding to clone types 7,



8, 9, 12, and 14 (Figure 5, Table 4) are also present. Type 15 produced a predicted T-RF of 39 bp. Ribotypes at 94, 134, 180, 199, 232, and 239 bp probably correspond to clone types 26, 23, 24, 20/21, 22, and 19/25, respectively (samples #3 and 4). All clones from samples #3 and #4 correspond to a ribotype resolved by the T-RFLP analyses as do most from samples #5 and #2. Clone types 11 and 13 from sample #2, however, appear to correspond to a very weak peak at the predicted 69-bp position (19 fluorescence units), not evident at the scale of display in Figure 5. Clone type 10, with a predicted T-RF of 202 bp from sample #2, lacked a detectable corresponding peak altogether.

Dendrograms using the Jaccard (presence or absence of common peaks) and Jaccard area-sensitive coefficients produced slightly different branch patterns and similarity values. The Jaccard area-sensitive representation was chosen for inclusion in Figure 6, since this calculation weights in favor of strong peaks and is thus likely to better represent this dataset (note the small number of strong peaks in Figure 5). In both analyses, the samples collected at the end of the experiment (samples #3 and #4) were most closely allied, occupying a common node with a cophenetic coefficient of 100. Jaccard and Jaccard area sensitive analyses disagreed on the assignment of samples #2 and #5, however. Whereas the Jaccard area sensitive treatment groups sample #2 with the borehole water and cartridge samples from the end of the experiment (samples #3 and #4), Jaccard analysis affiliates it with sample #5 (the biofilm sample).

### *16S rDNA Clone Libraries and Phylogeny*

Twenty-six distinct types were identified from among the 115 bacterial domain clones obtained from the borehole samples (Table 4). Clone type 18 was encountered most frequently, representing 36% of the biofilm (sample #5) clones, 41% of those in sample #2, and 62% and 50% of the clones from samples #3 and #4, respectively. Otherwise, rDNA sequences segregated into three assemblages corresponding to sample: a) an aerobic biofilm community, b) a transitional borehole water community, and c) a final borehole water community (Table 4). The biofilm sample (#5) and the early borehole water sample (#2) revealed proteobacterial clones. At the end of the equilibration period (samples #3 and #4) however, the proteobacterial clones had almost completely disappeared and a variety of deeply branching bacterial lineages emerged (Table 4). No archeal PCR products could be amplified from any of the associated samples. Eightyfour and 24 bacterial rDNA clones, respectively, were sequenced from comparative service and dolomite aquifer water samples with no sequences appearing in common with the borehole-associated samples (data not shown). A diversity of archaeal clones were recovered from service and dolomite water samples (Takai et al. 2001a).

The biofilm sample (#5) yielded seven clone types (1–6 and 18, Table 4). Types 1–6 were within the  $\alpha$ -subdivision of the *Proteobacteria* (Table 4, Figure 7). All clones except types 6 (also present in the cartridge material) and 18 were unique to this sample.

---

**FIGURE 4** SEM micrographs of a representative quartzite fragment recovered from the cartridge experiment. Bacterial colonization of the sand grains was heterogeneous (a), ranging from individual cells or microcolonies composed of a few cells (b) to a thin,  $\mu\text{m}$ -scale biofilm covering most of the mineral surface (c). Note the mineral surface is visible “through” the biofilm indicating that it is no more than a few micrometers thick. Bars equal 100  $\mu\text{m}$ , 20  $\mu\text{m}$ , and 20  $\mu\text{m}$ , respectively.

TABLE 4 Summary of clone groups and predicted ribotypes

Clone type	T-RF (bp)	General phylogenetic position of clone(s)	Sequence similarity to most closely related sequence in RDP or GenBank/EMBL databases	Number of clones				
				BH1 <sup>b</sup> (#2)	BH2 <sup>c</sup> (#3)	SC <sup>d</sup> (#4)	BF <sup>a</sup> (#5)	
1	39	$\alpha$ -Proteobacteria	96.0% <i>Phenylbacterium immobile</i> DSM 1986 <sup>e</sup> 96.0% <i>Afpia</i> genosp. 14 96.0% Env. clone (from soil) 5C2					1
2	39	$\alpha$ -Proteobacteria	94.0% <i>Rhodobium orientis</i> JCM 9337					2
3	39	$\alpha$ -Proteobacteria	96.1% <i>Roseovarius tolerans</i> DSM 11457 96.1% <i>Silicibacter lacuscaerulensis</i> ITI 1157					7
4	193	$\alpha$ -Proteobacteria	90.2% <i>Rhodospirillum rubrum</i>					1
5	39	$\alpha$ -Proteobacteria	90.6% <i>Rhodospirillum rubrum</i>					2
6	82	$\alpha$ -Proteobacteria	90.6% <i>Rhodospirillum rubrum</i>			2		1
7	219	$\beta$ -Proteobacteria	90.6% <i>Magnetospirillum gryphiswaldense</i> DSM 636					
8	219	$\beta$ -Proteobacteria	97.9% Env. clone (from Lake Soyang) SY6-23	2				
9	219	$\beta$ -Proteobacteria	98.6% Env. clone (from Columbia River) CRE-FL40	3				
10	202	$\beta$ -Proteobacteria	95.8% Env. clone (from Adirondack lake) ACK-C30	1				
11	69	$\beta$ -Proteobacteria	94.4% <i>Methylobacillus flagellatum</i> str. KT1	2				
12	217	$\beta$ -Proteobacteria	93.9% “ <i>Nitrosomonas oligotropha</i> ”	1				
13	69	$\beta$ -Proteobacteria	98.2% <i>Ideonella dechloratans</i> CCUG 30898	1				
14	207	$\beta$ -Proteobacteria	96.3% <i>Roseateles depolymerans</i> DSM 11813	1				
15	39	$\gamma$ -Proteobacteria	96.9% Env. clone (from rhizosphere) LRE13	1				
16	211	$\gamma$ -Proteobacteria	98.0% Env. clone (from rhizosphere) TBS12	1				
17	264	Gram-positive bacteria	99.9% <i>Marinobacter hydrocarbonoclasticus</i>	7				
18	264	Gram-positive bacteria	92.0% <i>Desulfotomaculum geothermicum</i> DSM 3669 92.9% <i>Desulfotomaculum thermosaprovorans</i>	14	2	18	14	8

18a	291	Gram-positive bacteria			1
19	238	Gram-positive bacteria	87.0% <i>Clostridium purinolyticum</i> ATCC 33906		1
20	199	Gram-positive bacteria	86.7% <i>Clostridium purinolyticum</i> ATCC 33906	2	
			86.7% <i>Clostridium thermolacticum</i> DSM 2911		
21	199	Gram-positive bacteria	84.3% <i>Desulfotomaculum geothermicum</i> DSM 3669		1
22	232	Gram-positive bacteria	87.4% <i>Geobacillus thermocatenulatus</i> DSM 730	1	1
23	134	Uncertain (deeply branching)	80.3% <i>Desulfotomaculum australicum</i> ACM 3917		1
			80.3% <i>Desulfotomaculum nigrificans</i> NCIMB 8395		
24	180	Uncertain (deeply branching)	84.8% <i>Geobacillus thermocatenulatus</i> DSM 730	2	
25	239	Uncertain (deeply branching)	80.3% <i>Geobacillus thermocatenulatus</i> DSM 730	4	9
26	94	Uncertain (deeply branching)	80.3% <i>Sphingomonas paucimobilis</i>		1
			78.4% <i>Geovibrio ferrireducens</i> str. PAL-1		

<sup>a</sup>Biofilm sample 5 November 1998.

<sup>b</sup>Borehole water 2 December 1998.

<sup>c</sup>Borehole water 3 February 1999.

<sup>d</sup>Cartridge material 4 February 1999.

<sup>e</sup>Genbank accession number.

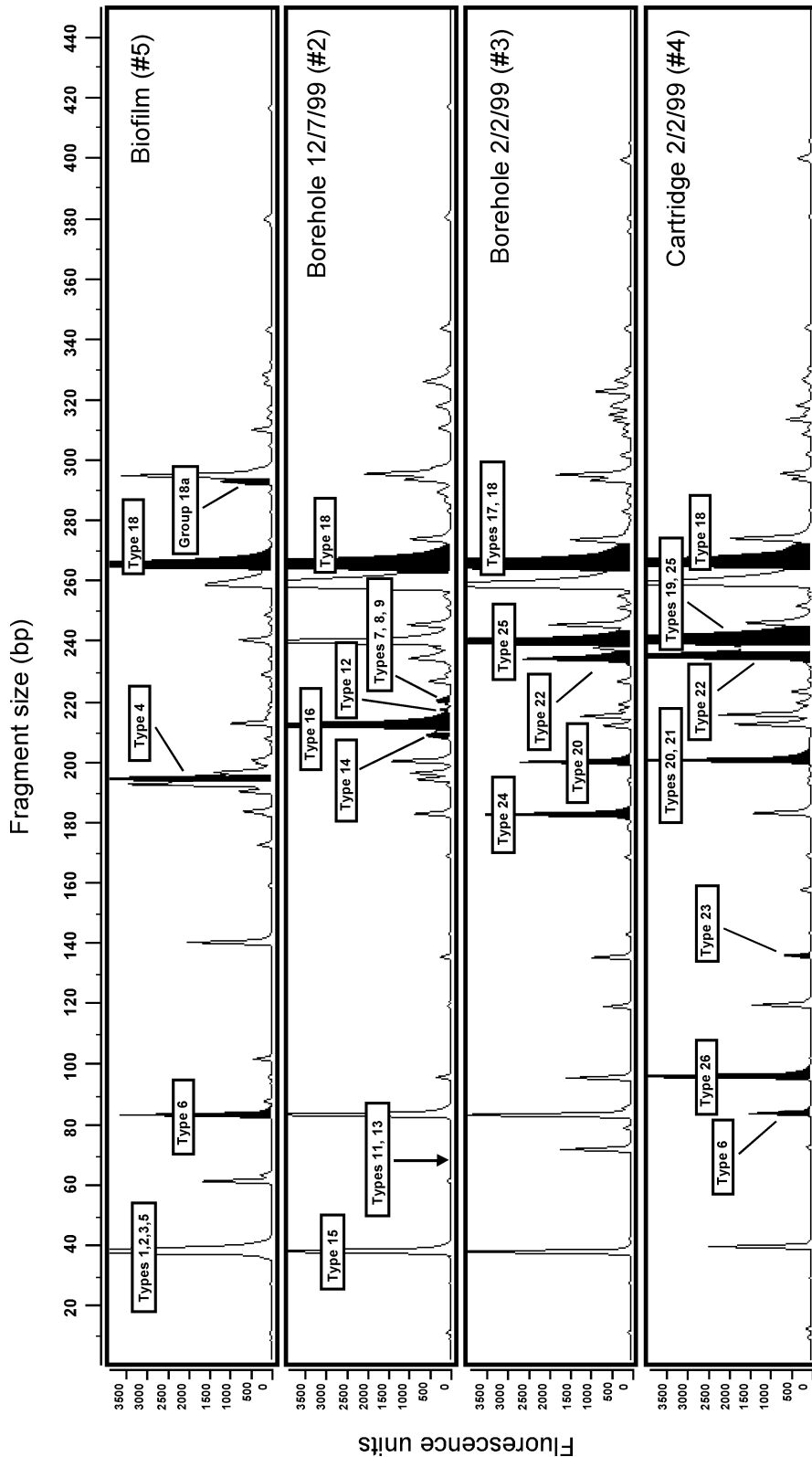


**FIGURE 5** Terminal Restriction Fragment profiles for borehole water and cartridge samples. Peak heights are in GeneScan fluorescence units. Time progression generally from top to bottom. T-RFs for which an apparent corresponding clone type exists in the appropriate library are blacked out and labeled. The arrow at the 69 bp position in panel #2 corresponds to a subtle peak (not visible at the scale of the figure, 19 fluorescence units) which may correspond to clone types 11 and 13. The strong, unlabeled peak at the 259 bp position was not represented by a potential clone type from any of the libraries.

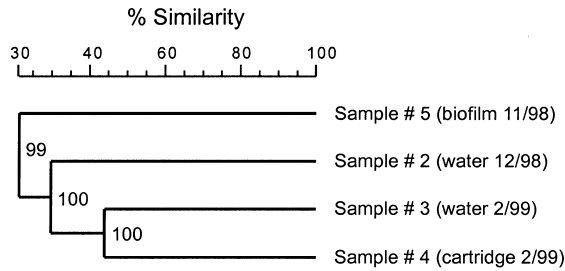


**FIGURE 6** Dendrogram generated from rDNA T-RF by the unweighted pair-group mean-average (UPGMA) method using the Jaccard area-sensitive coefficient. Cophenetic correlations appear at the nodes.

The rDNA library from sample #2 contained, in addition to type 18, eight types within the  $\beta$ -subdivision of the *Proteobacteria* (7–14) and two (15 and 16) within the  $\gamma$ -subdivision. Clone libraries derived from samples #3 and #4 were similar to each other, but distinct from the earlier samples (Table 4). Type 18 clones appeared in both samples and the closely related type 17 appeared in #3. All of the other clone types from these samples (19–26) are loosely affiliated with the low G+C Gram-positive bacteria (Figure 8). Types 22 and 25 were present in both samples, whereas types 17, 20, and 24 were unique to sample #3 and types 19, 21, 23, and 26 to sample #4 (Table 4).

Figures 7 and 8 resolve the phylogenetic positions of the *Proteobacteria*-like and the Gram-positive-like clones, independently. Two trees were required due to the great phylogenetic distances encompassed within the nonproteobacterial lineages. As shown in Figure 7, the unique biofilm clones fall within several  $\alpha$ -proteobacterial groups including the *Caulobacter* group, the *Rhizobiaceae*, the *Rhodobacter* group, and the *Rhodospirillaceae*. By contrast, the unique sample #2 clones fall entirely within the  $\beta$ - and  $\gamma$ -subdivisions of the *Proteobacteria* and affiliate with the *Methylophilus* group, the “Ammonia-oxidizing bacteria” group, the *Comamonadaceae*, the *Pseudomonadaceae*, and the *Alteromonadaceae* (Figure 7). Type 16 bears high sequence homology (99.9%) to *Marinobacter hydrocarbonoclasticus*.

Clone types 17 and 18, sharing 92% and 92.9% identity with *Desulfotomaculum geothermicum* and *Desulfotomaculum thermosapovorans*, respectively (Table 4), cluster with the *Desulfotomaculum* subgroup of the *Bacillus/Clostridium* group (Figure 8). Clones of types 19–26 exhibited less than 88% sequence identity to their nearest GenBank or RDP neighbor. Type 19 appears to be a deeply branching member of the subgroup *Clostridiaceae*. Types 20–26 are distributed throughout the low G+C Gram-positive bacteria but cannot be affiliated at the subgroup level with any specific known taxa. Types 20 and 21 establish a monophyletic branch outside the *Desulfotomaculum* subgroup of the *Bacillus/Clostridium* group. Type 22 also appears to be within the *Bacillus/Clostridium* group. Types 23, 24, and 25 branch very deeply within the *Bacillus/Clostridium* group. Type 26 appears to bear a weak phylogenetic relationship with the iron reducer (Caccavo et al. 1996), *Geovibrio ferrireducens*.

## Discussion

During the 2 months following the isolation of the borehole, shifts in microbial community structure occurred simultaneously with a slight decrease in salinity and increases in the pH,  $\text{Fe}^{+2}$ ,  $\text{SO}_4^{-2}$ , and DIC (Table 2). Whereas the changes in chemistry cannot be explained by

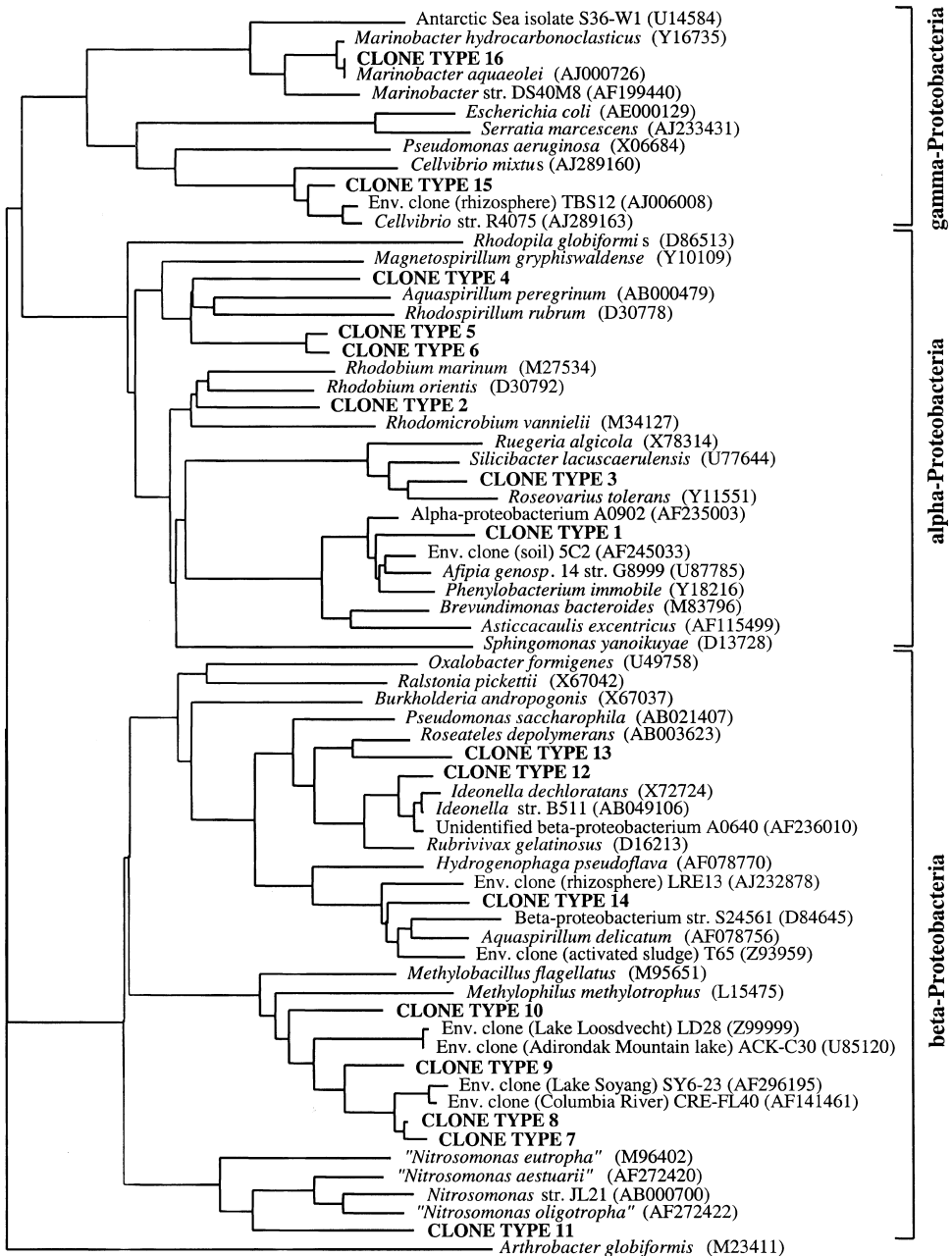


**FIGURE 7** Phylogenetic tree for proteobacterial 16S rDNA clones from the borehole environment (see Table 4), based on a distance matrix analysis. The PHYLIP program (Felsenstein 1995) was used to calculate distances by the method of Jukes and Cantor (1969), after which the Fitch option (Fitch and Margoliash 1967) was used to estimate phylogenies from distance matrix data. *Arthrobacter globiformis* was used as the outgroup. Scale bar represents 2 substitutions per 100 bases.

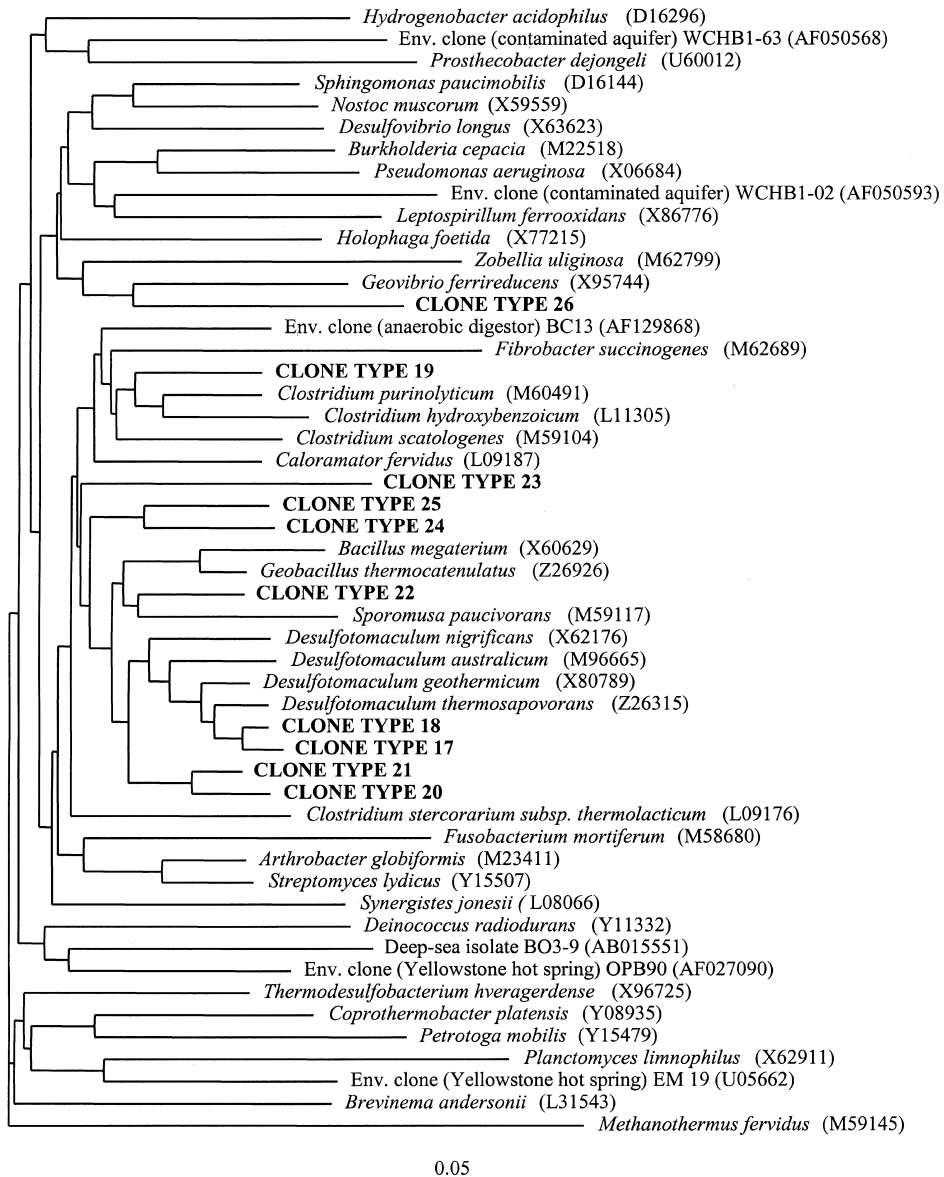


**FIGURE 8** Phylogenetic tree for Gram-positive and deeply branching 16S rDNA clones from the borehole environment (see Table 4), based on a distance matrix analysis and the same procedure used in Figure 7. The *Archaea*, *Methanothermus fervidus* was used as the outgroup. Individual group consensus sequences were aligned with their closest database match along with selected related organisms and one representative of each of the currently recognized bacterial phyla. Scale bar 5 represents substitutions per 100 bases.

the mixing with low salinity service water or dolomite water, they are readily modeled as microbially influenced shifts in redox reaction rates within the borehole itself. A variety of geochemical markers indicate that the borehole water is most likely representative of local formation waters. Stable isotopic composition,  $\delta^{18}\text{O}$  and  $\delta\text{D}$ , reflects the alteration of feldspar minerals to clay within the host Ventersdorp Supergroup under conditions of

low water-rock ratio (Duane et al. 1997) and low temperature (ca.  $<70^{\circ}\text{C}$ ), and implies a lengthy subsurface residence time. The high concentrations of He (Table 2) are likewise consistent with long subsurface residence times (Marine 1979). Analyses and modeling of noble gas isotopic compositions and  $^{36}\text{Cl}$  from the same borehole constrain the age of the water to lie between 4 and 52 Ma (Lippmann et al. 2001). Neither the  $\delta^{18}\text{O}$  nor the He gas concentration changed during the 2-month period, suggesting that changes in the microbial community are not due to changes in the source of the borehole water.

### ***Borehole Geochemistry and Geochemical Modeling***

The chemistry of the open borehole water is best explained as a steady-state kinetic equilibrium between sulfate reduction with organic matter and possibly  $\text{H}_2$  as the electron donors, and sulfide oxidation by atmospheric  $\text{O}_2$  with the mine  $\text{CO}_2$  acting as a pH buffer (Table 3). Upon isolation from the air, any residual dissolved  $\text{O}_2$  would have been consumed by microbial oxidation of  $\text{H}_2$ , organic matter, sulfide (Reactions 1, 2, and 3 in Table 3) or all three, and the pe would have decreased (Figure 2).  $\text{H}_2$  oxidation would have no effect on pH and would deplete the  $\text{H}_2$  in the absence of  $\text{H}_2$ -producing reactions. Oxidation of organic C would increase the DIC while decreasing the pH slightly. Sulfide oxidation, either via biotic or abiotic reactions, would increase sulfate concentrations and reduce the pH. Once the  $\text{O}_2$  had been depleted, the subsequent increase in  $\text{H}_2$  could reflect the actions of one or more biotic or abiotic pathways for generating  $\text{H}_2$ .

The increase in soluble iron ( $\text{Fe}^{+2}$ ) can best be attributed to anaerobic microbial processes where sulfide,  $\text{H}_2$ , or organic carbon are the electron donors and  $\text{Fe}^{+3}$  serves directly or indirectly as the electron acceptor (reactions 4, 5, and 6, respectively, Table 3) and where  $\text{Fe}^{+2}$  has not reacted with  $\text{HS}^-$  to form  $\text{FeS}$ . Potentially, reaction 4 can also explain the increase in sulfate, whereas reactions 5 and 6 would require an alternate source. The  $>1$  mmol of  $\text{H}^+$  ions consumed by all three reactions required to generate the 0.7 mmol of  $\text{Fe}^{+2}$  (Table 3) results in a final pH of 7.8 to 9.0 and a pe of  $-4.5$  to  $-5.8$ ; thus, a pH buffer is also required to explain the observed pH. The oxidation of  $\text{HS}^-$  coupled to the reduction of  $\text{Fe}^{+3}$ , when equilibrated with  $\text{CO}_2$ , yields a pH and pe comparable to that of the final borehole chemistry (reaction 7 in Table 3). The amount of sulfate generated by this reaction, however, is far less than observed and any further  $\text{Fe}^{+3}$  reduction would quickly lead to a  $\Delta\text{G}$  of zero. The slight decrease observed in the  $\delta^{34}\text{S}$  of  $\text{SO}_4^{2-}$  indicates that the oxidation of sulfide, which has a much lighter  $\delta^{34}\text{S}$  value, cannot be the principal sulfate source and indicates that reaction 7 is not responsible for the geochemical changes in the borehole.

The sulfate increase can be explained, however, by dissolution of gypsum (barite dissolution would have resulted in a Ba concentration higher than observed). The former is theoretically possible since the volume of water in the sealed borehole increased and would have submerged any crusts formed at the top of the old water levels. Alternatively, microbiological sulfur disproportionation, a physiological reaction that utilizes an intermediate oxidation state to yield both the fully oxidized and fully reduced state (Habicht et al. 1998), should be considered. Both thiosulfate and sulfite can be disproportionated by microbes (Habicht et al. 1998), while elemental sulfur requires the concomitant reduction of a metal to keep the sulfide concentration low (Thandrup et al. 1993). Microbial disproportionation can fractionate several different sulfur intermediates to generate both isotopically light sulfide ( $^{32}\text{S}$  enrichment) and isotopically heavy ( $^{34}\text{S}$  enrichment) sulfate as end products (Habicht et al. 1998).

Sulfate in the borehole system changed by about 0.5 per mil toward a lighter isotopic composition during the course of the experiment. If this shift resulted from disproportionation, then the sulfur intermediates were substantially lighter in isotopic composition than the

original sulfate pool. Given that the sulfate concentration doubled (from 0.579 to 1.16 mM) and the final  $\delta^{34}\text{S}$  of sulfate was 0.5 per mil lighter than the initial  $\delta^{34}\text{S}$  of sulfate, the isotopic composition of added sulfate must be 1 per mil lighter than initial sulfate. Reaction modeling was used to verify that oxidation of sulfide coupled to the reduction of  $\text{Fe}^{+3}$  fails to yield the observed pH, Eh, and  $\Delta G$  (Table 3) of the borehole system. Consequently, we infer partial oxidation of sulfide ( $\delta^{34}\text{S}$  of 1.4 ‰) to yield an intermediate sulfur species with an isotopic composition similar to that of the sulfide source (Habicht et al. 1998) as the most likely explanation for the concentration change and isotopic shift. The inferred intermediate sulfur species would be disproportionated to yield additional sulfate with an isotopic composition about 1‰ less than the initial sulfate, resulting in the observed negative shift in the final sulfate pool. Since initial  $\text{HS}^-$  concentrations were low, pyrite or monosulfide are inferred to be the sources of sulfide. Notably, a copious black precipitate was noted in the borehole prior to isolation. As oxidants within the borehole became depleted following isolation, sulfide oxidation would have ceased and production of sulfur intermediates would have ended. Consistent with this hypothesis, one measurement taken 2 years after the completion of this study (data not shown) revealed thiosulfate concentrations below detection limits.

Because of the increase in pH, the borehole became supersaturated with respect to calcite and siderite (Table 2). The precipitation of siderite during the  $\text{H}_2$ -oxidizing,  $\text{Fe}^{+3}$ -reducing reaction (Reaction 10 in Table 3) yields a pH and pe similar to that observed (Figure 2), but this coupled reaction predicts a decrease in DIC, not an increase as observed. Since microbes growing by disproportionation can be autotrophic, it is possible that disproportionation, if it occurred, may have served to introduce organic carbon into the system. When acetate oxidation coupled to  $\text{Fe}^{+3}$  reduction is combined with siderite equilibration (Reaction 12 in Table 3 and Figure 2), the modeled pH, pe, and DIC values match those in the final borehole sample. Correspondingly, the increase in inorganic carbon was accompanied by a decrease in the calculated  $\delta^{13}\text{C}$  of the  $\text{CO}_2$  in the borehole headspace from  $-20\text{‰}$  to  $-24\text{‰}$  PDB. This is consistent with organic matter acting as the electron donor. The  $\delta^{13}\text{C}$  of the DIC suggests that dissolved organic carbon was the principal electron donor for this reaction and that equilibration with the borehole headspace provided sufficient buffering capacity to moderate the increase in pH.

To summarize the geochemical analyses,  $\text{Fe}^{+3}$  reduction by acetate (Reactions 6 and 12 in Table 3) most accurately describes the final borehole chemistry where the pH is 7.4 and the pe is between  $-3$  and  $-4$ . This is because the  $\text{HCO}_3^-$  partially buffers the pH of the system. Additional buffering can result from  $\text{CO}_2$  gas in the borehole and/or carbonate precipitation. The oxidation of  $\text{H}_2$  by  $\text{Fe}^{+3}$  reduction coupled to equilibration with headspace  $\text{CO}_2$  also yield a pH, pe, and DIC comparable to that of the final borehole chemistry (Reaction 9 in Table 3). By contrast, the amount of pH buffering provided by acetate oxidation during sulfate reduction would be insufficient to prevent the pH from drifting upwards to 9, much greater than the measured value (Figure 2). Taken together, the observed sulfate increase and lack of increase in the  $\delta^{34}\text{S}$  of  $\text{SO}_4^{2-}$  are consistent with a decrease in the microbial  $\text{SO}_4^{2-}$  reduction rate upon isolation of the borehole.

### SEM

Bacterial colonization of the quartzite fragments occurred in a heterogeneous manner (Figure 4a) and did not appear to be controlled by  $\mu\text{m}$ -scale surface features (Figure 4b). Therefore, bacterial growth on these relatively inert quartzite surfaces is likely controlled by preferential flow paths “around” the fragments. The colonization and/or growth of bacteria on the mineral surfaces versus the low bacterial populations in the fluid phase (from

$2.5 \times 10^3$  cells/ml to  $3 \times 10^5$  cells/ml; determined by PLFA analysis) indicates that the mineral surface affords a competitive advantage for these bacteria in this oligotrophic environment. However, an unusual feature of the biofilm was the lack of extensive exopolymeric material (capsule) in association with cells or with the quartzite surfaces. The inability to form capsule and retain bacteria in the biofilm may be responsible for the thinness of the biofilm, which did not exceed a few  $\mu\text{m}$  (Figure 4c). Although bacteria can alter the chemical conditions at their surface, i.e., on the scale of nanoenvironments (Purcell 1992), this  $\mu\text{m}$ -scale biofilm is not deep enough to create a dramatic redox boundary within the biofilm, therefore, all of the bacteria in the cartridge were exposed to similar chemical conditions. Note, however, that the chemistry changed as biofilm developed, presumably due to colonization of the quartzite matrix, demonstrating bacterial control over groundwater chemistry versus bacteria simply responding to groundwater constituents. These observations suggest that fractures bearing groundwater should be targeted for analysis of subsurface bacteria where bacterial growth may be promoted at the mineral interface along groundwater flow paths.

### Microbial Community Structure

The 16S rDNA phylogeny, terminal restriction fragment (T-RFLP), and lipid biomarker (PLFA) analyses all revealed changes in microbial community structure. As indicated by these molecular measures, the biofilm community (#5) was distinct from those of the borehole and cartridge (#s 2, 3, 4), with only two (types 6 and 18) of 26 identified clone types in common with any (Table 4). Among the other clone types noted, the samples split nearly evenly along major phylogenetic lines (Table 4). In the aerobic biofilm sample (#5), all of the clones fell within the  $\alpha$ -*Proteobacteria*. This is supported in the PLFA dataset by a corresponding abundance (42 mol%) of monounsaturates, indicative of Gram-negative bacteria. In the borehole water sample (#2, collected shortly after the hole was sealed) the libraries were dominated by  $\beta$ - and  $\gamma$ -*Proteobacteria*. By the end of the experiment (samples #3 and #4), a community increasingly dominated by type 18 clones and containing a variety of deeply branching forms, most closely related to known Gram-positive bacteria and obligate anaerobes, developed. These shifts corresponded with a shift in lipid biomarker profiles towards PLFAs associated with similar organisms (Figure 3). Perhaps conspicuous by its absence is evidence indicative of  $\delta$ -*Proteobacteria* (e.g., *Desulfobrio* or *Geobacter*) in any samples relating to this system.

Terminally branched saturate PLFAs were indicative of Gram-positive bacteria and certain anaerobic bacteria (O'Leary and Wilkinson 1988; Kaneda 1991). Specific terminally branched saturates and branched monounsaturates can be associated with various sulfate-reducing bacteria such as *Desulfotomaculum* (Kohring et al. 1994). The most noteworthy was in i15:0, which increased from 0.79 mol% in the initial sampling to 15.0 mol% and 15.6 mol% in samples #3 and #4. In cultivated strains of *Desulfotomaculum*, *D. geothermicum*, *D. thermosapovorans*, and *D. putei*, this individual PLFA comprised 33%, 23%, and 15% to 22% of the total PLFA, respectively (Y. Liu et al. 1997; Kuever et al. 1999; Chang et al. 2001). Other PLFA biomarkers recognized as major fatty acid components associated with sulfate reducers were i17:1 $\omega$ 7 for *Desulfobrio* (Edlund et al. 1985; Vainshtein et al. 1992) and for the thermophilic subsurface isolate *D. putei* (Y. Liu et al. 1997), 10me16:0 for *Desulfobacter* (Edlund et al. 1985; Dowling et al. 1986), and 17:1 (especially 17:1 $\omega$ 6) for *Desulfobulbus* (Parkes and Calder 1985). However, i17:1 $\omega$ 7 and 17:1 were detected only in the February samples (#s 3 and 4, at ca. 4 and 0.5 mol%, respectively) and 10 me16 was only detected in the November and December samples (#s 2 and 5, at ca. 0.6 mol%).

Therefore, the shift in borehole microbial community structure was from a low-biomass and predominantly Gram-negative community to one of higher biomass and predominately Gram-positive with biomarkers indicating the presence of SRB.

The affiliations of clone types 17 and 18 with known sulfate-reducing bacteria of the genus *Desulfotomaculum* (Table 4, Figure 8, Fardeau et al. 1995; Stackebrandt et al. 1997) may be sufficiently robust to presume a physiological relationship. The prominence of these groups in the clone libraries and T-RFLP profiles taken together with the increase in terminally branched saturate and branched monounsaturate PLFAs such as i15:0 and i17:1 $\omega$ 7c (Figure 3) suggest high relative cell numbers from the beginning of the experiment. The collective physiological footprint of these organisms might thus be reflected in the borehole chemistry. It follows then that the large population of *Desulfotomaculum*-like organisms probably participated in the sulfate reduction noted early in the experiment. Given that the relative abundances of *Desulfotomaculum*-associated biomarkers and 16S rRNA genes increased (Figure 3, Table 4) following the shift to Fe<sup>+3</sup> reduction, these organisms likely used both Fe<sup>+3</sup> and SO<sub>4</sub><sup>-2</sup> as electron acceptors.

Consistent with this hypothesis, Tebo and Obraztsova have described *Desulfotomaculum reducens*, which couples the reduction of Fe<sup>+3</sup> to the oxidation of a variety of short chain acids and alcohols for growth (Tebo and Obraztsova 1998), the same general physiology predicted in the chemical model. Additionally, Niggemyer et al. describe metal-reducing physiology in stains of the closely related genus, *Desulfitobacterium* spp (Niggemyer et al. 2001). The emergence of Fe<sup>+3</sup> reduction where previously sulfate reduction was the dominant anaerobic process may reflect the submergence of previously corroded borehole casing surfaces after the system was isolated. Increasing water levels may have served to facilitate contact between bioavailable Fe<sup>+3</sup> and the microbial community. Under these circumstances, Fe<sup>+3</sup> may have been preferentially utilized, even in the presence of mM sulfate concentrations.

The success of *Desulfotomaculum*-like organisms in this environment is consistent with the known character of the genus, e.g., members are often halotolerant and moderately thermophilic (Stackebrandt et al. 1997). *Desulfotomaculum* spp. have been recovered from other subsurface habitats, such as oil production facilities (Rosnes et al. 1991; Tardy-Jacquenod et al. 1998), saline groundwaters in a geothermal heating plant (Daumas et al. 1988), and from deep terrestrial basins (Y. Liu et al. 1997). The closest RDP matches for clone types 17 and 18 are *D. geothermicum* (Daumas et al. 1988) and *D. thermosapovorans* (Fardeau et al. 1995). These species displayed temperature and salinity optima of 54°C and 50°C and of 3% and 3.5%, respectively. Still, given the many opportunities for the transfer of microbes into this system during and since the drilling of the borehole, origins are difficult to establish and endospores-forming SRB are thought to possess an advantage under unstable redox conditions (Widdell 1992; Kuever et al. 1999). Pedersen et al. reported that *D. nigrificans* (Campbell and Postgate 1965) survived in a sealed borehole for over one year when added to bentonite drilling mud (Pedersen et al. 2000). Thus, the occurrence of *Desulfotomaculum*-like SRB may be due to their survivability and capacity for the colonization of suitable habitats.

The numerically abundant clone type 16 from sample #2 proved nearly identical in sequence to the  $\gamma$ -proteobacterium, *Marinobacter hydrocarbonoclasticus* (Table 4, Gauthier et al. 1992). T-RFLP analysis revealed a prominent, corresponding ribotype at 211 bp (Figure 5, Table 4) that appeared only as a minor peak in the other samples. The transient nature of the *Marinobacter* bloom may be reflective of similarly ephemeral conditions shortly following isolation. Members of the *Marinobacter* group appear to possess an intrinsic tolerance to shifts in salinity, temperature, redox status, and nutrition (Gauthier et al.

1992; Huu et al. 1999), traits that would decline in value as the system approached steady state.

### ***Bacterial Populations at the End of the Experiment***

In the final sampling, the borehole had become highly reducing (pe of  $-3$ , Table 2). All of the molecular measures (Figures 3, 5, and 6, Table 4) indicated that the bacterial community structures of sample #3 and the in situ incubated quartzite fragments (sample #4) closely resembled one another but were distinct from the earlier samples. The relative peak intensities of the ribotypes corresponding to the newly appearing clones of types 19 to 26 all increased significantly in the later samples and with a few exceptions (Table 4), all were unique to the late samples. Terminally branched saturate and branched monoenoic PLFAs (both indicative of Gram-positive bacteria and certain anaerobes) likewise increased.

### **Conclusions**

Our data suggests that microbial community structure and the habitat itself underwent a gradual reequilibration with the deeply reducing native environment following exclusion from mine air influences. Chemical modeling and sulfur isotope analyses indicate a general shift from microbial sulfate reduction to  $\text{Fe}^{+3}$  reduction resulting from this treatment. Molecular methods recorded the coincident emergence of Gram-positive and deeply branching lineages. The PLFA and geochemical data showed a shift to Gram-positive, sulfate-reducing, and metal-reducing communities adapted to the changing geochemical conditions. The deep phylogenetic novelty of the lineages that appeared following borehole isolation suggests that this may be a habitat that has until now escaped the attention of those engaged in environmental assessments of microbial diversity. These unusual lineages may thus derive from the local deep subsurface and the borehole may represent a direct conduit into an extant, yet very old, fractured basalt microbial ecosystem.

### **References**

- Balkwill DL, Leach FR, Wilson JT, McNabb JF, White DC. 1988. Equivalence of microbial biomass measures based on membrane lipid and cell wall components, adenosine triphosphate, and direct counts in subsurface sediments. *Microbial Ecol* 16:73–84.
- Bligh EG, Dyer WJ. 1959. A rapid method of total lipid extraction and purification. *Can J Biochem Phys* 37:911–917.
- Boston PJ, Spilde MN, Northup DE, Melim LA, Soroka DS, Kleina LG, Lavoie KH, Hose LD, Mallory LM, Dahm CN, Crossey LJ, Schelble RT. 2001. Cave biosignature suites: microbes, minerals, and mars. *Astrobiol J* 1:25–55.
- Boschker HTS, Nold S, Wellsbury P, Bos D, deGraaf W, Parkes, RPJ, Cappenburg TE. 1998. Direct linking of microbial populations to specific biogeochemical processes by  $^{13}\text{C}$ -labelling of biomarkers. *Nature* 392:801–805.
- Brosius J, Palmer ML, Kennedy PJ, Noller HF. 1979. The complete nucleotide sequence of the ribosomal 16-S RNA from *Escherichia coli*. Experimental details and cistron heterogeneities. *Eur J Biochem* 100:399–410.
- Caccavo Jr. F, Coates JD, Rossello-Mora RA, Ludwig W, Schleifer KH, Lovley DR, McInerney MJ. 1996. *Geovibrio ferrireducens*, a phylogenetically distinct dissimilatory Fe(III)-reducing bacterium. *Arch Microbiol* 165:370–376.

- Campbell LL, Postgate JR. 1965. Classification of the endospore-forming sulfate reducing bacteria. *Bacteriol Rev* 29:359–363.
- Cary SC, Cottrell MT, Stein JL, Camacho F, Desbruyeres D. 1997. Molecular identification and localization of filamentous symbiotic bacteria associated with the hydrothermal vent annelid *Alvinella pompejana*. *Appl Environ Microbiol* 63:1124–1130.
- Chang Y-J, Peacock AD, Long PE, Stephen JR, McKinley JP, Macnaughton SJ, Hussain AKMA, Saxton AM, White DC. 2001. Diversity and characterization of sulfate-reducing bacteria in groundwater at a uranium mill tailings site. *Appl Environ Microbiol* 67:3149–3160.
- Chapelle FH, O'Neill K, Bradley PM, Methe BA, Ciufo SA, Knobel LL, Lovley DR. 2002. A hydrogen-based subsurface microbial community dominated by methanogens. *Nature* 415:312–315.
- Colwell FS, Onstott TC, Dilwiche ME, Chandler D, Fredrickson JK, Yao Q- J, McKinley JP, Boone DR, Griffiths R, Phelps TJ, Ringelberg D, White DC, LaFreniere L, Balkwill D, Lehman RM, Konisky J, Long PE. 1997. Microorganisms from deep, high temperature sandstones: constraints on microbial colonization, *FEMS Microbiol Rev* 20:425–435.
- Daumas S, Cord-Ruwisch R, Garcia JL. 1988. *Desulfotomaculum geothermicum* sp. nov., a thermophilic, fatty acid-degrading, sulfate-reducing bacterium isolated with H<sub>2</sub> from geothermal ground water. *Antonie Van Leeuwenhoek* 54:165–178.
- Delany JM, Lundeen SR. 1990. The LLNL thermochemical database. Lawrence Livermore National Laboratory Report, UCRL-21658.
- DeLong EF. 1992. Archaea in coastal marine environments. *Proc Natl Acad Sci USA* 89:5685–5689.
- Dowling NJE, Widdle F, White DC. 1986. Phospholipid ester-linked fatty acid biomarkers of acetate-oxidizing sulfate-reducers and other sulfide-forming bacteria. *J Gen Microbiol* 132:1815–1826.
- Duane MJ, Pigozzi, G, Harris C. 1997. Geochemistry of some deep gold mine waters from the Western Portion of the Witwatersrand Basin, South Africa. *J African Earth Sci* 24:105–123.
- Eaton AD, Clesceri LS, Greenberg AE. 1998. In: Standard Methods for the Examination of Water and Wastewater, 20th ed. Philadelphia, PA: American Public Health Association, American Water Works Association, Water Pollution Control Federation. p 4-103-4-112.
- Edlund A, Nichols PD, Roffey R, White DC. 1985. Extractable and lipopolysaccharide fatty acid and hydroxy fatty acid profiles from *Desulfovibrio* species. *J Lipid Res* 26:982–988.
- Fardeau ML, Ollivier B, Patel BK, Dwivedi P, Ragot M, Garcia JL. 1995. Isolation and characterization of a thermophilic sulfate-reducing bacterium, *Desulfotomaculum thermosapovorans* sp. nov. *Int J Syst Bacteriol* 45:218–221.
- Felsenstein J. 1985. Confidence limits on phylogenies: an approach using the bootstrap. *Evolution* 39:783–791.
- Felsenstein J. 1993. PHYLIP (Phylogeny inference package), version 3.5c, University of Washington, Seattle.
- Findlay RH, Dobbs FC. 1993. Quantitative description of microbial communities using lipid analysis. In: Kemp PF, Sherr BF, Sherr EB, Cole JJ. editors. *Handbook of Methods in Aquatic Microbial Ecology*. Boca Raton, FL: Lewis Publishers Inc. p 271–284.
- Fitch WM, Margoliash E. 1967. Construction of phylogenetic trees. *Science* 155:279–284.
- Fredrickson JK, Onstott TC. 1996. Microbes deep inside the Earth. *Sci Am* 275:68–73.
- Gauthier MJ, Lafay B, Christen R, Fernandez L, Acquaviva M, Bonin P, Bertrand JC. 1992. *Mari-nobacter hydrocarbonoclasticus* gen. nov., sp. nov., A new, extremely halotolerant, hydrocarbon-degrading marine bacterium. *Int J Syst Bacteriol* 42:568–576.
- Giovannoni SJ. 1991. The polymerase chain reaction. In: Stackebrandt E, Goodfellow M. editors. *Nucleic Acid Techniques in Bacterial Systematics*. New York: John Wiley & Sons. p 177–203.
- Guckert JB, Antworth CP, Nichols PD, White DC. 1985. Phospholipid, ester-linked fatty acid profiles as reproducible assays for changes in prokaryotic community structure of estuarine sediments. *FEMS Microbiol Ecol* 31:147–158.
- Gutell RR. 1994. Collection of small subunit (16S- and 16S-like) ribosomal RNA structures. *Nucleic Acids Res* 17:3502–3507.

- Habicht KS, Canfield DE, Rethmeier J. 1998. Sulfur isotope fractionation during bacterial reduction and disproportionation of thiosulfate and sulfite. *Geochim Cosmochim Acta* 62:2585–2595.
- Haveman S, Pedersen K, Ruotsalainen P. 1999. Distribution and metabolic diversity of microorganisms in deep igneous rock aquifers of Finland. *Geomicrobiol J* 16:277–294.
- Huu NB, Denner EBM, Ha Dang TC, Wanner G, Stan-Lotter H. 1999. *Marinobacter aquaeolei* sp. nov., a halophilic bacterium isolated from a Vietnamese oil-producing well. *Int J Syst Bacteriol* 49:367–375.
- Johnson KM, Seiburth JM, Williams PJB, Brandstrom L. 1987. Coulometric TCO<sub>2</sub> analyses for marine studies: automation and calibration. *Mar Chem* 21:117–133.
- Jukes TH, Cantor CR. 1969. Evolution of protein molecules. In: Munro HN, editor. *Mammalian Protein Metabolism*. New York: Academic Press. p 21–132.
- Kaneda T. 1991. Iso- and anteiso-fatty acids in bacteria: biosynthesis, function, and taxonomic significance. *Microbiol Rev* 55:28.
- Kieft TL, Kovacik WP Jr, Ringelberg DB, White DC, Haldeman DL, Amy PS, Hersman LE. 1997. Factors limiting microbial growth and activity at a proposed high-level nuclear repository, Yucca Mountain, Nevada. *Appl Environ Microbiol* 63:3128–3133.
- Kohring LL, Ringelberg DB, Devereux R, Stahl DA, Mittelman MW, White DC. 1994. Comparison of phylogenetic relationships based on phospholipid fatty acid profiles and ribosomal RNA sequence similarities among dissimilatory sulfate-reducing bacteria. *FEMS Microbiol Lett* 119:303–308.
- Kotelnikova S, Pedersen K. 1998. Distribution and activity of methanogens and homoacetogens in deep granitic aquifers at Äspö hard rock laboratory, Sweden. *FEMS Microbiol Ecology* 26:121–134.
- Kuever J, Rainey FA, Hippe H. 1999. Description of *Desulfotomaculum* sp. *Groll* as *Desulfotomaculum gibsoniae* sp. nov. *Int J Syst Bacteriol* 49:1801–1808.
- Lane DJ. 1991. 16S/23S rRNA sequencing. In: Stackenbrandt E, Goodfellow M, editors. *Nucleic Acid Techniques in Bacterial Systematics*. Chichester, United Kingdom: Wiley. p 115–175.
- Lippmann J, Stute M, Moser DP, Hall J, Lin L, Ward JA, Slater GF, Onstott TC, Schlosser P. 2001. Noble gas study on deep mine waters, South Africa. *Eos Trans. AGU*, 82: Fall Meet. Suppl, Abstract H22C-0370.
- Liu WT, Marsh TL, Cheng H, Forney LJ. 1997. Characterization of microbial diversity by determining terminal restriction fragment length polymorphisms of genes encoding 16S rRNA. *Appl Environ Microbiol* 63:4516–4522.
- Liu Y, Karnauchow TM, Jarrell KE, Balkwill DL, Drake GR, Ringelberg D, Clarno R, Boone DR. 1997. Description of two new thermophilic species of *Desulfotomaculum*, *Desulfotomaculum putei* sp. nov. from the deep terrestrial subsurface and *Desulfotomaculum luciae* sp. nov. from a hot spring. *Int J Syst Bacteriol* 47:615–621.
- Maidak BL, Cole JR, Parker CT Jr, Garrity GM, Larsen N, Li B, Lilburn TG, McCaughey MJ, Olsen GJ, Overbeck R, Pramanik S, Schmidt TM, Tiedje JM, Woese CR. 1999. A new version of the RDP (Ribosomal Database Project). *Nucleic Acids Res* 27:171–173.
- Marine IW. 1979. The use of helium to estimate groundwater velocities for studies of geologic storage of radioactive waste, *Wat Resour Res* 15:1130–1135.
- Nichols DS, Olley J, Garda H, Brenner, RR, McMeekin TA. 2000. Effect of temperature and salinity stress on growth and lipid composition of *Shewanella gelidimarina*. *Appl Environ Microbiol* 66:2422–2429.
- Nicolaysen LO, Hart RJ, Gale NH. 1981. The Vredefort radioelement profile extended to supracrustal strata at Carletonville, with implications for continental heat flow. *J Geophysical Res* 86:10653–10661.
- Niggemyer A, Spring S, Stackenbrandt E, Rosenzweig RF. 2001. Isolation and characterization of a novel As(V)-reducing bacterium: implications for arsenic mobilization and the genus *Desulfotomaculum*. *Appl Environ Microbiol* 67:5568–5580.
- O’Leary WM, Wilkinson SG. 1988. Gram-positive bacteria. In: Ratledge C, Wilkinson SG, editors. *Microbial Lipids*. London: Academic Press. p 117–201.
- Onstott TC, Phelps TJ, Colwell FS, Ringelberg D, White DC, Boone DR, McKinley JP, Stevens TO, Balkwill DL, Griffin T, Kieft T. 1998. Observations pertaining to the origin and ecology of

- microorganisms recovered from the deep subsurface of Taylorsville Basin, Virginia. *Geomicrobiol J* 15:353–385.
- Orphan VJ, Taylor LT, Hafenbradl D, Delong EF. 2000. Culture-dependent and culture-independent characterization of microbial assemblages associated with high-temperature petroleum reservoirs. *Appl Environ Microbiol* 66:700–711.
- Parkes RJ, Calder AG. 1985. The cellular fatty acids of three strains of *Desulfobulbus*, a propionate-utilizing sulfate-reducing bacterium. *FEMS Microbiol Ecol* 31:361–363.
- Pedersen K, Hallbeck L, Arlinger J, Erlandson AC, Jahromi N. 1997. Investigation of the potential for microbial contamination of deep granitic aquifers during drilling using 16S rRNA gene sequencing and culturing methods. *J Microbiol Methods* 30:179–192.
- Pedersen K, Motamedi M, Karnland O, Sandén T. 2000. Cultivability of microorganisms introduced into a compacted bentonite clay buffer under high-level radioactive waste repository conditions. *Eng Geol* 58:149–161.
- Purcell E. 1992. Life at low Reynolds number. *Amer J Phy* 45:3–11.
- Rosnes JT, Torsvik T, Lien T. 1991. Spore-forming thermophilic sulfate-reducing bacteria isolated from North Sea oil field waters. *Appl Environ Microbiol* 57:2302–2307.
- Sambrook J, Fritsch EF, Maniatis T. 1989. *Molecular cloning: a laboratory manual*. Cold Spring Harbor, NY: Cold Spring Harbor Laboratory Press.
- Sokal RR, Michener CD. 1958. A statistical method for evaluating systematic relationships. *Univ Kans Sci Bull* 38:1409–1438.
- Sokal RR, Sneath PHA. 1963. *Principles of numerical taxonomy*. San Francisco: WH Freeman & Company. p 169–210.
- Stackebrandt E, Sproer C, Rainey FA, Burghardt J, Pauker O, Hippe H. 1997. Phylogenetic analysis of the genus *Desulfotomaculum*: evidence for the misclassification of *Desulfotomaculum guttoideum* and description of *Desulfotomaculum orientis* as *Desulfosporosinus orientis* gen. nov., comb. nov. *Int J Syst Bacteriol* 47:1134–1139.
- Stevens TO, McKinley JP, Fredrickson JK. 1993. Bacteria associated with deep, alkaline, anaerobic groundwaters in southeast Washington. *Microb Ecol* 25:35–50.
- Stahl DA, Amann R. 1991. Development and application of nucleic acid probes in bacterial systematics. In: Stackebrandt E, Goodfellow M, editors. *Nucleic Acid Techniques in Bacterial Systematics*. New York: John Wiley & Sons, Inc. p 205–248.
- Takai K, Moser DP, DeFlaun M, Onstott TC, Fredrickson JK. 2001a. Archaeal diversity in deep South African gold mine waters. *Appl Environ Microbiol* 67:5750–5760.
- Takai K, Moser DP, Onstott TC, Spoelstra N, Piffner SM, Dohnalkova A, Fredrickson JK. 2001b. *Alcaliphilus auruminator* gen. Nov., sp. Nov., an extremely alkaliphilic bacterium isolated from a deep South African gold mine. *Int J Syst Bacteriol* 51:1245–1256.
- Tardy-Jacquenod C, Magot M, Patel BK, Matheron R, Caumette P. 1998. *Desulfotomaculum halophilum* sp. nov., a halophilic sulfate-reducing bacterium isolated from oil production facilities. *Int J Syst Bacteriol* 48:333–338.
- Tebo BM, Obratsova AY. 1998. Sulfate-reducing bacterium grows with Cr(VI), U(VI), Mn(IV), and Fe(+3) as electron acceptors. *FEMS Microbiol Lett* 162:193–198.
- Thamdrup B, Finster K, Hansen JW, Bak F. 1993. Bacterial disproportionation of elemental sulfur coupled to chemical reduction of iron or manganese. *Appl Environ Microbiol* 59:101–108.
- Tunlid A, Ringelberg D, Phelps TJ, Low C, White DC. 1989. Measurement of phospholipid fatty acids at picomolar concentrations in biofilms and deep subsurface sediments using gas chromatography and chemical ionization mass spectrometry. *J Microbiol Meth* 10:139–153.
- Vainshtein M, Hippe H, Kroppenstedt RM. 1992. Cellular fatty acid composition of *Desulfovibrio* species and its use in classification of sulfate-reducing bacteria. *Syst Appl Microbiol* 15:554–566.
- White DC, Davis WM, Nickels JS, King JD, Bobbie RJ. 1979. Determination of the sedimentary microbial biomass by extractable lipid phosphate. *Oecologia* 40:51–62.
- White, DC, Pinkart HC, Ringelberg DB. 1997. Biomass measurements: biochemical approaches. In: Hurst CJ, Knudsen GR, McInerney MJ, Stetzenbach LD, Walter MV, editors. *Manual of Environmental Microbiology*. Washington, DC: American Society for Microbiology. p 91–101.

- White DC, Ringelberg DB. 1998. Signature lipid biomarker analysis. In: Burlage RS, Atlas R, Stahl DA, Geesey G, Saylor G, editors. *Techniques in Microbial Ecology*. New York: Oxford University Press. p 255–272.
- Widdell F. 1992. The genus, *Desulfotomaculum*. In: Balows A, Truper HG, Dwarkin M, Harder W, Schleifer K-H, editors. *The Prokaryotes*. New York: Springer-Verlag. p 1792–1799.
- Zobell CE. 1946. Studies of redox potential of marine sediments. *Bull Am Assoc Petrol Geol* 30:477–513.

Copyright of Geomicrobiology Journal is the property of Taylor & Francis Ltd and its content may not be copied or emailed to multiple sites or posted to a listserv without the copyright holder's express written permission. However, users may print, download, or email articles for individual use.